

Portland State University

PDXScholar

Geology Faculty Publications and Presentations

Geology

7-2023

Effects of Landslides on Terrestrial Carbon Stocks With a Coupled Geomorphic-Biologic Model: Southeast Alaska, United States

Adam M. Booth

Portland State University, boothad@pdx.edu

Brian Buma

University of Colorado, Denver

S. Nagorski

University of Alaska-Southeast

Follow this and additional works at: https://pdxscholar.library.pdx.edu/geology_fac



Part of the [Geology Commons](#)

Let us know how access to this document benefits you.

Citation Details

Booth, A. M., Buma, B., & Nagorski, S. (2022). Effects of landslides on terrestrial carbon stocks with a coupled geomorphic-biologic model: Southeast Alaska, United States. *Journal of Geophysical Research: Biogeosciences*, e2022JG007297.

This Article is brought to you for free and open access. It has been accepted for inclusion in Geology Faculty Publications and Presentations by an authorized administrator of PDXScholar. Please contact us if we can make this document more accessible: pdxscholar@pdx.edu.



RESEARCH ARTICLE

10.1029/2022JG007297

Key Points:

- Coupled landslide-carbon model shows landslides boost C stocks by sequestering C in deposits and creating space for new C to accumulate
- Size of the boost increases with landslide frequency, from ~1% at an areal frequency of $\sim 10^{-4}$ yr $^{-1}$ to ~6.5% by a frequency of 10^{-3} yr $^{-1}$
- Landslides in temperate rainforests are likely a net C sink with respect to the atmosphere and a buffer against increasing atmospheric CO $_2$ levels

Supporting Information:

Supporting Information may be found in the online version of this article.

Correspondence to:

A. M. Booth,
boothad@pdx.edu



Citation:

Booth, A. M., Buma, B., & Nagorski, S. (2023). Effects of landslides on terrestrial carbon stocks with a coupled geomorphic-biologic model: Southeast Alaska, United States. *Journal of Geophysical Research: Biogeosciences*, 128, e2022JG007297. <https://doi.org/10.1029/2022JG007297>

Received 18 NOV 2022

Accepted 2 JUN 2023

Effects of Landslides on Terrestrial Carbon Stocks With a Coupled Geomorphic-Biologic Model: Southeast Alaska, United States

A. M. Booth¹ , B. Buma^{2,3}, and S. Nagorski⁴ 

¹Department of Geology, Portland State University, Portland, OR, USA, ²Department of Integrative Biology, University of Colorado-Denver, Denver, CO, USA, ³Environmental Defense Fund, Boulder, CO, USA, ⁴Department of Natural Sciences, University of Alaska-Southeast, Juneau, AK, USA

Abstract Landslides influence the global carbon (C) cycle by facilitating transfer of terrestrial C in biomass and soils to offshore depocenters and redistributing C within the landscape, affecting the terrestrial C reservoir itself. How landslides affect terrestrial C stocks is rarely quantified, so we derive a model that couples stochastic landslides with terrestrial C dynamics, calibrated to temperate rainforests in southeast Alaska, United States. Modeled landslides episodically transfer C from scars to deposits and destroy living biomass. After a landslide, total C stocks on the scar recover, while those on the deposit either increase (in the case of living biomass) or decrease while remaining higher than if no landslide had occurred (in the case of dead biomass and soil C). Specifically, modeling landslides in a 29.9 km² watershed at the observed rate of 0.004 landslides km⁻² yr⁻¹ decreases average living biomass C density by 0.9 tC ha⁻¹ (a relative amount of 0.4%), increases dead biomass C by 0.3 tC ha⁻¹ (0.6%), and increases soil C by 3.4 tC ha⁻¹ (0.8%) relative to a base case with no landslides. The net effect is a small increase in total terrestrial C stocks of 2.8 tC ha⁻¹ (0.4%). The size of this boost increases with landslide frequency, reaching 6.5% at a frequency of 0.1 landslides km⁻² yr⁻¹. If similar dynamics occur in other landslide-prone regions of the globe, landslides should be a net C sink and a natural buffer against increasing atmospheric CO $_2$ levels, which are forecast to increase landslide-triggering precipitation events.

Plain Language Summary Landslides are a natural process, often triggered by rainfall, that removes soil and forest cover from steep slopes and deposits them in valleys. Those soils and vegetation contain large amounts of carbon that has been removed from the atmosphere by photosynthesis. Landslides and carbon are therefore related, but it has not previously been determined whether the net effect of landslides is to release carbon back to or sequester additional carbon from the atmosphere. Our work, focused on temperate rainforests in southeast Alaska, indicates that landslides sequester additional carbon from the atmosphere by burying existing carbon in deposits and providing space for new carbon to accumulate on landslide scars. The amount of additional carbon sequestration increases as landslides occur more frequently. As climate change leads to more extreme rainfall events in forested parts of the world, such as southeast Alaska, more landslides are expected to occur. Therefore, increased landsliding may partially offset some of the elevated atmospheric carbon dioxide levels that drive landslide-triggering extreme weather events in the first place, in a newly identified feedback loop.

1. Introduction

Geological and meteorological extreme events, such as earthquakes and storms, are important components of the geologic carbon (C) cycle. Landslides triggered by these events transfer C in biomass, soil, and near-surface bedrock from hillslopes to rivers, where it can then be transported to and buried in depocenters as particulate organic carbon (POC) (Croissant et al., 2021; Frith et al., 2018; Hilton, Galy, Hovius, et al., 2008; Hilton, Galy, & Hovius, 2008; Wang et al., 2016). That buried POC can remain sequestered from the atmosphere for geologic timescales (~millions of years), while the much more rapid recovery of vegetation and soils (~centuries to millennia) sequesters additional C from the atmosphere, suggesting that extreme events may be long-term C sinks. However, increased oxidative weathering of exposed rocks and decomposition of mobilized soils could dampen or counteract this potential sink effect in some settings (Bufe et al., 2021; Emberson et al., 2016, 2018). Nevertheless, the global flux of POC from the continents to the oceans is ~ 110 – 230 MtC yr $^{-1}$, of which ~ 40 – 80 MtC yr $^{-1}$ is buried in ocean sediments, comparable to the rate of C sequestration due to silicate weathering, and

© 2023 The Authors.

This is an open access article under the terms of the [Creative Commons Attribution-NonCommercial License](https://creativecommons.org/licenses/by/4.0/), which permits use, distribution and reproduction in any medium, provided the original work is properly cited and is not used for commercial purposes.

therefore likely plays a similar role in the drawdown of atmospheric CO₂ over geologic time (Bianchi et al., 2018; Galy et al., 2007; Hilton, 2017; Hilton & West, 2020).

More generally, erosive processes also redistribute terrestrial C within the landscape, thereby affecting C fluxes as well as the spatial pattern and size of the terrestrial C reservoir itself (Berhe et al., 2007, 2008; Billings et al., 2019; Doetterl et al., 2016; Yoo et al., 2005, 2006). In this study, we define terrestrial C as that which is contained in soil and biomass (living and dead). Erosion generally detaches, transports, and then deposits C at downslope locations (Lal, 2019). During detachment and transport, C that was previously protected can be exposed to enhanced decomposition, thereby decreasing terrestrial C over the timescale of detachment and transport. However, regrowth of vegetation at the eroding site, that is, dynamic replacement, and deposition of C at downslope locations with longer C residence times both contribute to longer term sequestration of C from the atmosphere (Berhe et al., 2007; Rosenbloom et al., 2006). Deposition sites are important C sinks because soils are typically deeper than at eroding sites and therefore can contain more C, while decomposition is also slowed due to deeper burial, protection in aggregates, and wetter conditions (Berhe et al., 2005, 2012; Doetterl et al., 2012; Yoo et al., 2006). Therefore, the relative importance of these C sources or sinks varies depending on the spatial and temporal scale of analysis (Van Oost & Six, 2023). For short periods of time (~years–decades), enhanced decomposition of soil C during detachment and transport can dominate over dynamic replacement, making erosion a net C source to the atmosphere (Lal, 2019; Ran et al., 2014). Over longer periods of time (~centuries or more), dynamic replacement at eroded sites and reduced decomposition rates at sites of deposition can dominate, making erosion a net C sink (Van Oost & Six, 2023). Considering these longer periods of time, erosion may globally be a net C sink, sequestering ~1 GtC yr⁻¹ (Berhe et al., 2007; Smith et al., 2001; Stallard, 1998), about an order of magnitude greater than POC burial or silicate weathering fluxes. Most of this previous work has focused on surficial soil erosion, especially of agricultural lands, and little has focused on landslides in natural, forested settings (Billings et al., 2019; Dialynas et al., 2016). We hypothesize that landslides in forests should be an effective C sink because detachment and transport happen quickly (~minutes), they bury C more deeply than surficial erosion, and they mobilize and bury biomass in addition to soil (Clark et al., 2016; Hilton et al., 2011; Johnson et al., 2000; Lancaster et al., 2003; Ramos Scharrón et al., 2012; Vascik et al., 2021; Wang et al., 2016; West et al., 2011).

Although the theoretical basis for erosion's influence on the C cycle is clear, determining how the magnitude and direction (sink or source) of that effect explicitly depend on the frequency of erosive events, their spatial distribution across a landscape, and their cumulative effects over different timescales has rarely been addressed quantitatively (Doetterl et al., 2016). Only a few studies have coupled geomorphic process-based models of erosion (*sensu* Dietrich et al., 2003) with carbon flux models (Billings et al., 2019; Dialynas et al., 2016; Rosenbloom et al., 2001, 2006; Yoo et al., 2005, 2006), and none of those have addressed landslides in carbon-dense temperate rainforests. One challenge is the wide gaps in scale among different modeling efforts. For the terrestrial C cycle, global scale models typically do not include physical transport of C across a landscape and group C into just a few different reservoirs, necessarily averaging over fine-scale details (Luo et al., 2015, 2017; Manzoni & Porporato, 2009). More detailed models that include effects of soil aggregates, moisture, and depth on C fluxes tend to be site specific, require large amounts of fieldwork to calibrate, and have often focused on agricultural lands (Doetterl et al., 2016). Erosion models are focused on the movement of sediment, rather than C, which further complicates their coupling with C cycle models. Nonetheless, process-based models of soil erosion and C fluxes applied to natural settings have shown that erosion systematically affects the residence times and spatial distribution of soil C within a landscape (Dialynas et al., 2016; Rosenbloom et al., 2006; Yoo et al., 2006).

In this study, we expand coupled, process-based modeling of erosion and the terrestrial C cycle to landslide-prone forested hillslopes. Our novel model combines stochastic landsliding with the terrestrial C cycle and is straightforward to calibrate with a landslide inventory and measured terrestrial C stocks and/or fluxes. After deriving the model, we calibrate it to a study site in southeast Alaska with one of the largest terrestrial C densities in the world. The model predicts that landslides there systematically increase total terrestrial C density by intermittently transferring C from reservoirs with relatively short C residence times (biomass) to that with a longer residence time (soil) at deposition sites, while new biomass C subsequently accumulates. Over the range of landslide frequencies documented at the study site, the magnitude of this effect is modeled to monotonically increase with landslide frequency, suggesting a negative feedback whereby increases in atmospheric CO₂ increase precipitation extremes and landslide frequency, which subsequently removes CO₂ from the atmosphere.

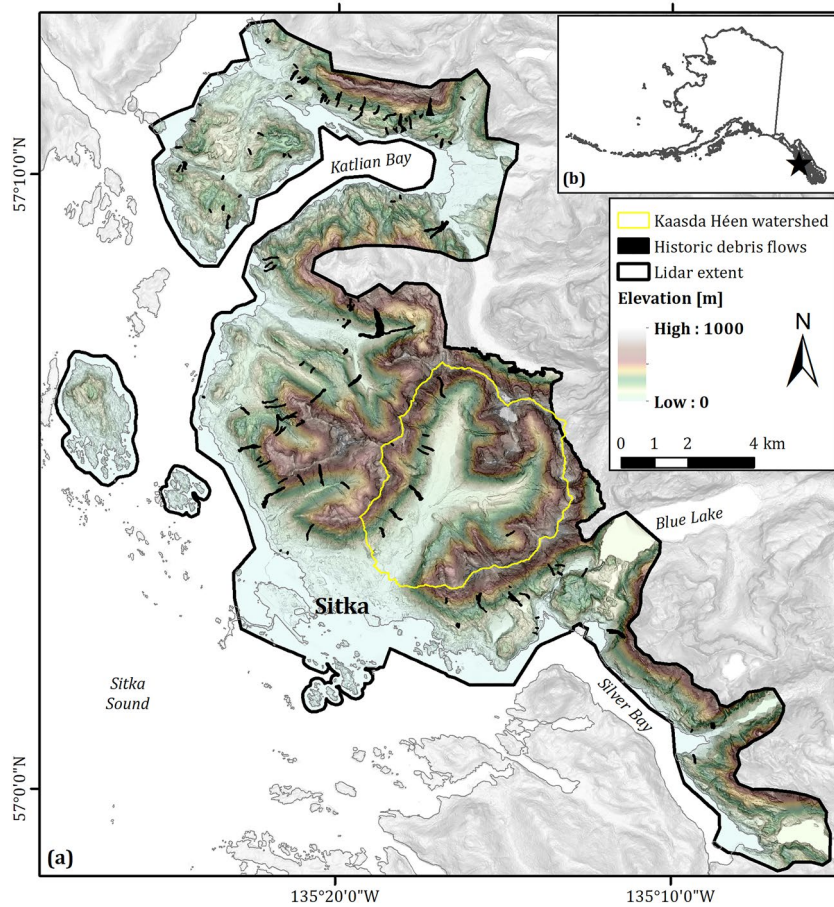


Figure 1. (a) Map of Sitka study area, and (b) its location within Alaska, United States (black star). Historic debris flows (black filled polygons) within the lidar extent (solid black line, elevations shown in color) were used to calibrate the landslide model. Landsliding and the terrestrial C cycle were modeled in the Kaasda Héen (Indian River) watershed (solid yellow line).

2. Study Site: Sitka, Alaska, United States

Southeast Alaska experiences ~ 0.002 landslides $\text{km}^{-2} \text{yr}^{-1}$ (Vascik et al., 2021) in steep, glacially sculpted terrain that is widely covered by old-growth temperate rainforests, making it an ideal site to investigate interactions between landslides and the terrestrial C cycle in a setting that has been minimally modified by humans. This study is focused on the area surrounding Sitka, Alaska (Figure 1), where the necessary data for calibrating the model are available (airborne lidar, a landslide inventory, and maps of terrestrial C density). Sitka has a mild, wet, maritime climate with average high temperatures above freezing at sea level year-round and >2 m of annual precipitation (Shulski & Wendler, 2007). Much of that precipitation occurs as storms with high wind speeds and rainfall rates, which are fed by atmospheric rivers in the northern Pacific Ocean and often trigger landslides (Booth et al., 2020; Gomi et al., 2004; Johnson et al., 2000; Sharma & Déry, 2020; Swanston et al., 1991; Vascik et al., 2021). The climate of the region has been relatively stable for the past 7,500 years, and fire has been rare (Gavin et al., 2003; Hansen & Engstrom, 1996; Veblen & Alaback, 1996).

The study area is underlain by Mesozoic sedimentary, metasedimentary, metavolcanic, and intrusive volcanic rocks of the Baranof Accretionary Complex and Wrangellia Terrane, parts of an accreted volcanic arc complex (Gehrels & Berg, 1992; Karl et al., 2015). Pleistocene glaciation has sculpted the bedrock into broad, steep-sided valleys and fjords, with the most recent glaciers beginning to retreat ~ 14.6 ka (Praetorius et al., 2016). Glaciation also left behind a thin layer of till up to elevations of $\sim 1,000$ m, which is overlain by ~ 1 m thick Late Pleistocene tephra that were erupted from the Mt. Edgumbe volcanic field, located ~ 25 km west of Sitka (Begét & Motyka, 1998; Riehle, 1996; Riehle et al., 1984). Contacts between bedrock and till, till and tephra, and layers within the tephra serve as failure planes for shallow landslides, which often mobilize into debris flows, the

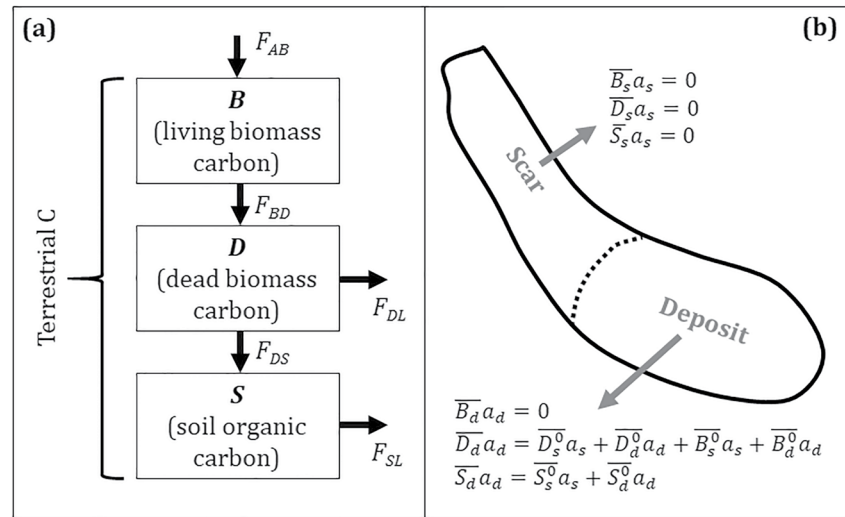


Figure 2. (a) Terrestrial C cycle model diagram in which B , D , and S are the sizes of each C reservoir (tC ha^{-1}) at a given point in the landscape, and F_{ij} is the C flux from pool i to pool j ($\text{tC ha}^{-1} \text{yr}^{-1}$) at that point, where A refers to the atmosphere, and L refers to generalized losses. (b) Diagram illustrating the modeled effects of a landslide on terrestrial C stocks immediately after the landslide occurred. Bars indicate the mean, a is area, the subscript s indicates the landslide scar, the subscript d indicates the deposit, and the superscript 0 indicates the C density immediately prior to the landslide. The landslide removes all C from the scar and transfers it to the deposit, while also converting all living biomass to dead biomass.

most common type of mass-movement in the study area (Booth et al., 2020; Patton et al., 2022). These shallow landslide-initiated debris flows strip soil and biomass from steep initiation sites high on hillslopes and deposit that material in valley bottoms or low order streams, where C is accumulated in lowland soils or exported to the Pacific Ocean (Vascik et al., 2021). Debris flows in the region tend to have limited runout, likely caused by interactions between large woody debris in the flow front with standing trees in the runout zone (Booth et al., 2020; Johnson et al., 2000).

The perhumid temperate rainforests of southeast Alaska are a globally significant terrestrial C reservoir, containing ~ 2.8 GtC in an area of $70,000 \text{ km}^2$, which is $\sim 0.1\%$ of global terrestrial C in just $\sim 0.05\%$ of the ice-free global land area (Houghton et al., 1990; Leighty et al., 2006). Soil is the region's largest terrestrial C reservoir with an average of 302 tC ha^{-1} in the upper 1 m (McNicol et al., 2019). Non-soil biomass (living and dead) averages 178 tC ha^{-1} over the entire region, including sparsely vegetated alpine areas, but is frequently $300\text{--}400 \text{ tC ha}^{-1}$, with some areas exceeding 700 tC ha^{-1} , in lower elevation forested areas (Buma et al., 2016; Buma & Thompson, 2019). Dead biomass makes up $\sim 20\%$ of total biomass (Leighty et al., 2006). In unmanaged forests in the region, total new C accumulation in living biomass has been balanced by mortality within measurement error over recent decades, suggesting biomass C density is broadly near steady state (Barrett, 2014). However, individual patches of forest have measurably lost or gained C density, with gains occurring mainly on north-facing aspects to the north of our study area, and losses occurring mainly on south-facing aspects to the south of our study area (Buma & Barrett, 2015). At the latitude of Sitka, gains have approximately balanced losses.

3. Methods

3.1. Model Development

We designed our model to explicitly link physical transport of C across the landscape driven by landslides with in-place C fluxes among living biomass, dead biomass, and soil C reservoirs (Figure 2). Modeled landslides episodically move terrestrial C downslope and change living biomass to dead biomass. The model deliberately strikes a balance between detailed, site-specific models and more general global C cycle models so that it can be readily calibrated with available data.

3.1.1. Stochastic Landslide Model

The goal of the landslide model is to efficiently produce landslides that individually have realistic geometries and collectively produce realistic spatial patterns and size distributions. This approach is a compromise between

physics-based, computationally expensive models (e.g., those reviewed in McDougall (2017)) and simpler empirical runout models (e.g., those reviewed in Rickenmann (1999)). Overall, we take a Monte Carlo approach in which we randomly sample from empirical distributions of landslide initiation locations, sizes, and runout properties to simulate a population of synthetic landslides over time. All landslide analyses and modeling were carried out on a bare earth, lidar-derived digital elevation model (DEM) upsampled to 5-m resolution with linear interpolation (Daanen et al., 2020).

For each model run, a series of landslide events is first defined by randomly sampling the number of landslides per event from an exponential distribution,

$$P(n) = \lambda e^{-\lambda n}, \quad (1)$$

where P is the probability of the number of landslides per event, n , and λ is a parameter that controls the shape of the distribution. Equation 1 generally captures the observations that landslides tend to occur in specific events, such as individual storms, and that events involving large numbers of landslides are rare compared to events with small numbers of landslides (Guthrie & Evans, 2004; Martin et al., 2002). Events are created until the total number of landslides gives a specified landslide frequency when averaged over the duration of the model run. Each event is then assigned to a random time during the model run.

To simulate each event, landslide initiation sites are sampled from a previously determined distribution of landslide susceptibility. We used the susceptibility map of Buma and Johnson (2015), which was derived from six topographic variables: slope, wind exposure, drainage area, topographic position index, terrain index, and presence or absence of hydric soils. Although vegetation was not explicitly included in determining landslide susceptibility, biomass density in the region is also dependent on similar topographic variables (Buma & Thompson, 2019), so effects of vegetation are implicitly incorporated in the susceptibility map. We linearly interpolated that 30-m resolution map to 5-m resolution for consistency with the lidar DEM and so that susceptibility smoothly varied across the landscape. Landslide areas were similarly sampled from the observed distribution of landslide areas in the study area (Figure S1a in Supporting Information S1).

From each initiation site, the model then simulates landslide runout by first routing flow to all downslope DEM cells with a multiple flow direction (MFD) algorithm, where the fractional flow is weighted by the slope between cells (Freeman, 1991). The fraction of flow each cell receives from its upslope neighbors is defined as the “influence,” to which thresholds can be applied to produce a discrete flow extent (Richardson & Karlstrom, 2019). We imposed two criteria to define the planform geometry of each simulated landslide: (a) influence must exceed a threshold, and (b) runout length, measured along the path of steepest descent, must be less than a threshold. Within each simulated landslide polygon, the one-third of cells with the smallest slopes are then defined as the deposit, and the two-thirds with the greatest slopes are designated the scar, based on field, lidar, and aerial photo interpretations. Although other two-dimensional empirical landslide runout models exist (e.g., LAHARZ (Iverson et al., 1998; Schilling, 1998) or DLFOWZ (Berti & Simoni, 2007, 2014)), our approach better captured runout geometry on quasi-planar slopes with both confined and unconfined flow conditions as well as multi-threaded runout paths, both of which were relatively common at the study site.

Last, to explicitly couple the landslide and terrestrial C models, each simulated landslide transfers all C in the scar to the deposit, and converts all living biomass to dead biomass (Figure 2b). Each landslide therefore (a) resets living biomass C to zero within its entire extent, (b) resets dead biomass and soil C to zero within its scar, and (c) increases both soil and dead biomass C in the deposit. In reality, landslides typically retain some soil and biomass in their scar area and do not destroy all the living biomass in their entire runout path, but those amounts are generally small compared to the bulk transfer of sediment and biomass from scar to deposit. Since the model distinguishes the scar and deposit based on slope, some patches of soil and dead biomass C are retained in isolated, low slope patches at high elevations, while the majority of the C is transferred to a main deposit at low elevations, mimicking this behavior to some extent (Movie S1).

3.1.2. Terrestrial Carbon Cycle Model

The terrestrial C model is a pool-and-flux model with three C reservoirs: living biomass (B), dead biomass (D), and soil (S) (Figure 2). Reservoirs other than these, such as the atmosphere, oceans, marine sediments, rivers, and bedrock, are not explicitly modeled, but the three terrestrial C reservoirs gain C from or lose C to those reservoirs through generalized fluxes that encompass one or more processes. Specifically, the living biomass

pool takes in C from the atmosphere through net primary productivity (F_{AB} in Figure 2a) and moves C to the dead biomass pool through tree mortality and accumulation of forest floor litter (F_{BD}). The dead biomass pool moves C to the soil pool if stabilized as soil organic C (SOC) (F_{DS}), or loses C through microbial respiration or erosion and transport in rivers (F_{DL}). The soil pool similarly loses C through respiration as well as erosion and transport of POC and dissolved organic carbon (DOC) in rivers (F_{SL}). Fire is largely absent in the coastal temperate rainforests of the region, so is not explicitly included in these fluxes (Gavin et al., 2003; Veblen & Alaback, 1996).

The rate of change of C in each pool is given by the difference between C fluxes into and out of the pool, leading to a system of coupled equations:

$$\frac{dB}{dt} = F_{AB} - F_{BD}, \quad (2a)$$

$$\frac{dD}{dt} = F_{BD} - F_{DL} - F_{DS}, \quad (2b)$$

$$\text{and } \frac{dS}{dt} = F_{DS} - F_{SL}, \quad (2c)$$

where F_{IJ} indicates the C flux from pool I to pool J . The subscript A refers to the atmosphere, while the subscript L refers to general losses of terrestrial C. As in other pool-and-flux models for the terrestrial C cycle (Luo et al., 2015, 2017; Manzoni & Porporato, 2009), we posit that the magnitudes of the fluxes are functions of the sizes of the relevant C pools:

$$\frac{dB}{dt} = (k_1 - k_2 B) - k_3 B, \quad (3a)$$

$$\frac{dD}{dt} = k_3 B - k_4 D - k_5 D, \quad (3b)$$

$$\text{and } \frac{dS}{dt} = k_5 D - k_6 S, \quad (3c)$$

where k_i are parameters that in general may vary as a function of space or time. In Equation 3a, k_1 is the initial net rate of living biomass C accumulation when $B = 0$ ($\text{tC ha}^{-1} \text{yr}^{-1}$), and k_2 is a rate constant (yr^{-1}) that characterizes the reduction in net primary productivity as B increases. The rate constant k_3 is equal to the fraction of the living biomass pool that is lost to the dead biomass pool per unit time. In Equation 3b, k_4 and k_5 are rate constants describing the fractions of the dead biomass pool that are lost or transferred to the soil pool, respectively, per unit time. The remaining rate constant, k_6 , in Equation 3c is the fraction of soil C lost per unit time.

Assuming temporally constant values for the parameters k_i , steady-state solutions to Equation 3 are then

$$B_{ss} = \frac{k_1}{k_2 + k_3}, \quad (4a)$$

$$D_{ss} = \frac{k_3}{k_4 + k_5} B_{ss}, \quad (4b)$$

$$\text{and } S_{ss} = \frac{k_5}{k_6} D_{ss}, \quad (4c)$$

where the subscript SS indicates steady state. The solutions to Equation 3 for the initial conditions $B(t = 0) = B_0$, $D(t = 0) = D_0$, and $S(t = 0) = S_0$ are

$$B(t) = B_{ss} + (B_0 - B_{ss})e^{-(k_2+k_3)t}, \quad (5a)$$

$$D(t) = D_{ss} + \beta e^{-(k_2+k_3)t} + (D_0 - D_{ss} - \beta)e^{-(k_4+k_5)t}, \quad (5b)$$

$$\text{and } S(t) = S_{ss} + \frac{k_5 \beta}{k_6 - k_2 - k_3} e^{-(k_2+k_3)t} + \frac{k_5(D_0 - D_{ss} - \beta)}{k_6 - k_4 - k_5} e^{-(k_4+k_5)t} + \gamma e^{-k_6 t}, \quad (5c)$$

$$\text{where } \beta = \frac{k_3(B_0 - B_{ss})}{-k_2 - k_3 + k_4 + k_5}, \quad (5d)$$

$$\text{and } \gamma = S_0 - S_{ss} - k_5 \left(\frac{\beta}{k_6 - k_2 - k_3} + \frac{D_0 - D_{ss} - \beta}{k_6 - k_4 - k_5} \right), \quad (5e)$$

which we use to calculate C densities as a function of time. When and where a landslide occurs, it resets B_0 , D_0 , and C_0 as depicted in Figure 2b, and then Equation 5 governs subsequent terrestrial C evolution.

3.2. Model Calibration

To calibrate the landslide model we used a population of 123 historic shallow landslides that mobilized into debris flows that occurred within the airborne lidar data extent (Figure 1). We downloaded georeferenced landslide shapefiles from the Tongass National Forest Landslide Inventory, maintained by the U. S. Department of Agriculture Forest Service (2018). That inventory was based primarily on interpretation of historic aerial photographs from 1929 to 2016. Polygons included the entire landslide (i.e., they did not distinguish between scar and deposit), and we analyzed landslides mapped as debris torrents, debris slides, and debris avalanches, which are more generally known as debris flows (Varnes, 1978). The frequency-magnitude distribution of landslide areas from the inventory is typically right-skewed (Malamud et al., 2004) and well fit by a log-normal distribution ($\mu = 8.34$, $\sigma = 1.22$; Figure S1a in Supporting Information S1). The modal landslide size given by the peak of the log-normal fit is 880 m², while the smallest and largest landslides in the study area are 100 m², and 156,000 m², respectively.

For runout parameters, we created an influence map for each landslide with the MULTIFLOW algorithm (Richardson & Karlstrom, 2019), routing flow downslope from the highest elevation DEM cell of each landslide polygon. We then determined the best-fit combination of influence and runout length thresholds that minimized an error index, that is, the threat score or critical success index, defined as the intersection divided by the union of predicted and mapped landslide areas (Booth et al., 2009; Carrara et al., 1992). Best-fit runout length, L , was significantly (>95% confidence) positively correlated with landslide area, A , such that $L = 1.4A^{0.59}$, and best-fit influence threshold, I , was significantly negatively correlated with landslide area such that $I = 12.1A^{-0.78}$ (Figures S1b and S1c in Supporting Information S1). We used those power-law fits to assign runout length and influence thresholds to each modeled landslide given its area. More generally, our thresholding approach produced qualitatively realistic landslide geometries that captured a wide range in landslide sizes, aspect ratios, and geometries (Figure S2 in Supporting Information S1).

We defined the model domain as the Kaasda Héen (Indian River) watershed upstream of Sitka, which has no history of timber harvest or road building. The watershed experienced nine landslides between 1929 and 2016 in 29.9 km² (4×10^{-3} landslides km⁻² yr⁻¹). There were too few historic landslides grouped into specific events to quantitatively calibrate the distribution of landslides per event (Equation 1). However, no more than three new landslides appeared in any historic aerial photograph, so we assumed $\lambda = 2$, which ensured that >99% of simulated events had three or fewer landslides.

To calibrate the C model, we used previously determined reservoir sizes and parameters in Equation 4 to solve for the remaining unknown parameters (Table 1). Specifically, we used the Buma and Thompson (2019) biomass C density map to determine B_{ss} and D_{ss} in each model grid cell, and the McNicol et al. (2019) soil C density map to determine S_{ss} . Buma and Thompson (2019) estimated biomass C density in 30 m pixels using 1,491 Forest Inventory and Analysis (FIA) plots in southeast Alaska, while McNicol et al. (2019) estimated soil C density in 90.5 m pixels using a compiled database of 1,300 soil profile descriptions from southeast Alaska and British Columbia. Although average biomass C stocks in southeast Alaska have been increasing over recent decades due to warming climate, those gains have been concentrated to the north of our study area (Buma & Barrett, 2015). Assuming that modern C densities are representative of long-term, steady-state values is therefore a reasonable first-order approximation for our Holocene timescale simulations, also considering that climate has been relatively stable in the study area for the past 7,500 years (Hansen & Engstrom, 1996). Including landslides in our model then simulates changes to C densities relative to this assumed steady state. Both maps were downscaled using linear interpolation to the same 5 m grid as the lidar DEM. Within the Kaasda Héen watershed modeling extent (Figure 1), median steady-state living biomass C density was 214 tC ha⁻¹, and median dead biomass density was 53 tC ha⁻¹, assuming 20% of total biomass was dead (Leighty et al., 2006). Median soil C density was 425 tC ha⁻¹.

Table 1
Carbon Model Parameters and Steady-State Fluxes

Parameter	Value		Units	Source(s)
	Median (25th, 75th percentile)			
B_{ss}	214 (120, 289)		tC ha ⁻¹	Buma and Thompson (2019)
D_{ss}	53 (30, 72)		tC ha ⁻¹	Buma and Thompson (2019), Leighty et al. (2006)
S_{ss}	425 (392, 460)		tC ha ⁻¹	McNicol et al. (2019)
k_1	3		tC ha ⁻¹ yr ⁻¹	DeMars (2000), Leighty et al. (2006)
k_2	0.009 (0.006, 0.020)		yr ⁻¹	Equation 4a
k_3	0.005		yr ⁻¹	Equation 4b
k_4	0.01		yr ⁻¹	Harmon et al. (2005)
k_5	0.01		yr ⁻¹	Harmon et al. (2005)
k_6	0.0012 (0.0007, 0.0016)		yr ⁻¹	Equation 4c
F_{AB}	1.0 (0.6, 1.4)		tC ha ⁻¹ yr ⁻¹	Equation 3a
F_{BD}	1.0 (0.6, 1.4)		tC ha ⁻¹ yr ⁻¹	Equation 3a
F_{DA}	0.5 (0.3, 0.7)		tC ha ⁻¹ yr ⁻¹	Equation 3b
F_{DS}	0.5 (0.3, 0.7)		tC ha ⁻¹ yr ⁻¹	Equation 3b
F_{SA}	0.5 (0.3, 0.7)		tC ha ⁻¹ yr ⁻¹	Equation 3c

For the constants, we set $k_1 = 3$ tC ha⁻¹ yr⁻¹ based on the typical initial rate of biomass C accumulation in even-aged hemlock-Sitka spruce stands following logging, fire, and blowdown throughout southeast Alaska (DeMars, 2000; Leighty et al., 2006). Rates of downed coarse wood volume loss for Sitka spruce in southeast Alaska are 1.9% yr⁻¹, with roughly half of that loss due to microbial respiration (F_{DL}) and the other half to soil (F_{DS}) (Harmon et al., 2005). Since downed coarse wood is the largest constituent of the dead biomass pool, we assumed that rate represents the entire dead biomass pool, such that $k_4 = k_5 = 0.01$ yr⁻¹. The remaining constants have not been measured in southeast Alaska, so we calculated them using Equation 4. For biomass, k_2 varied spatially and had a median value of 0.009 yr⁻¹, and k_3 was spatially constant with a value of 0.005 yr⁻¹, giving biomass C accumulation curves consistent with that of Leighty et al. (2006), in which steady-state biomass C was attained by ~350 years following disturbance. For soil, k_6 varied spatially and had a median value of 0.0012 yr⁻¹.

At steady state, our calibrated model parameters imply $F_{AB} = F_{BD} = 1.0$ tC ha⁻¹ yr⁻¹ on average. For comparison, Barrett (2014) calculated C fluxes throughout southeast Alaska over decadal time scales from FIA data and estimated a live tree C accumulation rate of 0.66–0.80 tC ha⁻¹ yr⁻¹ and a downed wood C accumulation rate of 0.44–0.69 tC ha⁻¹ yr⁻¹. Those short-term, regional estimates are not necessarily representative of steady state at our specific study site, but are nonetheless similar to the modeled fluxes, suggesting reasonable calibration. The calibration also implies that $F_{DL} = F_{DS} = F_{SL} = 0.5$ tC ha⁻¹ yr⁻¹ on average. Present day DOC fluxes, a component of F_{SL} , range from 0.02 to 0.61 tC ha⁻¹ yr⁻¹ in forested watersheds throughout southeast Alaska (Edwards et al., 2021; Hood et al., 2020) and from 0.24 to 0.38 tC ha⁻¹ yr⁻¹ to the south in coastal British Columbia (Oliver et al., 2017). Otherwise, soil C fluxes have not been measured directly in southeast Alaska, but C accumulation rates for volcanic soils in general are 0.04–0.8 tC ha⁻¹ yr⁻¹ (Arnalds, 2013), and rates of 0.12–0.34 tC ha⁻¹ yr⁻¹ have been measured at Mt. Shasta in the Pacific Northwest of North America (Lilienfein et al., 2003; Sollins et al., 1983). The similar magnitudes of DOC fluxes, soil C accumulation rates, and modeled fluxes also suggests reasonable calibration, and that DOC fluxes are an important component of terrestrial C losses in the region.

3.3. Model Implementation

To roughly approximate the post-glacial evolution of terrestrial C stocks, we assumed initial conditions of $B_0 = D_0 = S_0 = 0$ throughout the entire model domain, and simulated 14,500 years for each model run. We first analyzed a base case with no landslides (Equation 5) to characterize the residence and response times for each C pool. We then ran the model with landslide frequency tuned to the historical frequency in the Kaasda Héen watershed. Acknowledging uncertainties in the calibrated model parameters, we re-ran this model 100 times

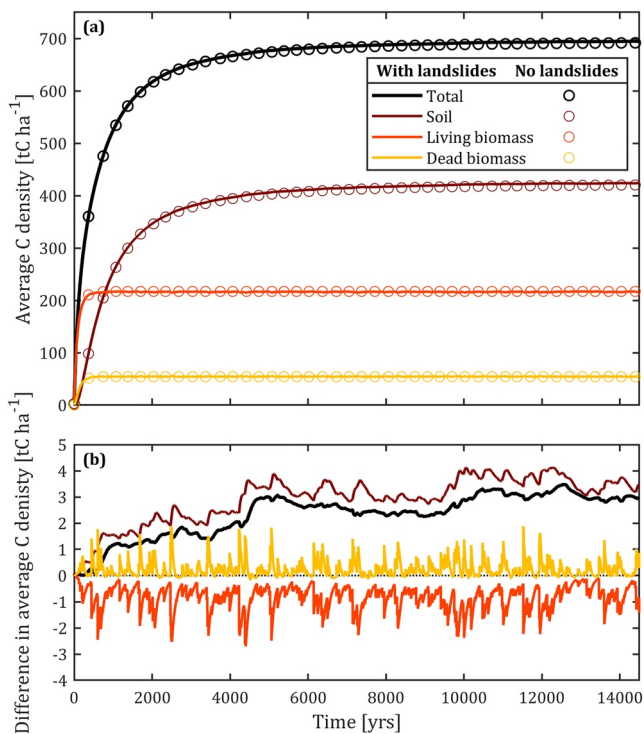


Figure 3. (a) Modeled average C densities versus time for the base case of no landslides (open circles) and the case with landslide frequency tuned to the historic rate in the Kaasda Héén watershed (solid lines), with terrestrial C model parameters as given in Table 1. (b) Landslide-induced change in average C density relative to the base case versus time.

with random, normally distributed relative errors with a standard deviation of $\pm 15\%$ added to each terrestrial C model parameter to characterize the average behavior and its variability. Last, we ran the model over a wide range of landslide frequencies that have been documented at forested sites throughout the world to determine the sensitivity of C stocks to landslide frequency.

4. Results

4.1. Base Case: Terrestrial C Model With No Landslides

In the absence of landslides, mean steady-state C densities in the Kaasda Héén watershed (Figure 1) are 217, 54, 427, and 699 tC ha⁻¹ for living biomass, dead biomass, soil, and total terrestrial C, respectively. Mean C turnover times at steady state, defined as the size of each C reservoir divided by the steady-state C flux to or from the reservoir (Mudd & Yoo, 2010), are therefore 214 years for living biomass, 53 years for dead biomass, and 843 years for soil. From the assumed initial condition of no terrestrial C on the landscape 14,500 years ago, biomass C initially begins to accumulate at a rate of 3 tC ha⁻¹ yr⁻¹ as set by k_1 , then rolls over with a response time of 87 years, defined here as the time to reach within e^{-1} (37%) of its steady-state value (Figure 3a). As a fraction of that living biomass is converted to dead biomass, the dead biomass C pool increases gradually at first, reaches a maximum net accumulation rate of 0.29 tC ha⁻¹ yr⁻¹ at 60 years, and then rolls over with a response time of 149 years. Soil C initially accumulates slowly due to low input from dead biomass, reaches a maximum net accumulation rate of 0.36 tC ha⁻¹ yr⁻¹ at 280 years, and then gradually rolls over with a response time of 1,122 years.

Total terrestrial C initially tracks living biomass C, then increases more rapidly than living biomass C as the dead biomass and soil C pools begin to accumulate. As the biomass C pools approach their steady-state sizes by a few hundred years, total C rolls over more sharply and after about 500 years increases at essentially the same rate (within 5%) as soil C. The response time of total C is 609 years.

4.2. Coupled Landslide-Carbon Model Tuned to Kaasda Héén Watershed

Including landslides in the model at the historic rate in the Kaasda Héén watershed causes average C densities to fluctuate and systematically differ from those of the base case (Figure 3, Movie S1). To illustrate the effects of landslides on C densities, we first analyze a hypothetical single landslide with an area of two grid cells, one as the scar and the other as the deposit, that occurs 100 years into the model run in an area with average C model parameter values (Figure 4). In the scar, the landslide resets all C densities to zero, reducing B , D , S , and total C density by 163, 26, 10, and 199 tC ha⁻¹, respectively, which are the base case C densities at that time. Following the landslide, all C densities begin to increase again, approaching their steady-state values, but remain less than in the base case for at least the next 200 years. In contrast, on the deposit only B is reset to zero, while D and S increase due to the additional C transported from the scar and the conversion of living biomass to dead biomass. Specifically, B decreases by 163 tC ha⁻¹, D increases by 351 tC ha⁻¹, S increases by 10 tC ha⁻¹, and total C increases by 199 tC ha⁻¹. After the landslide, D decreases because it has been elevated to well above its steady-state density, and it remains greater than in the base case. As D decreases, it drives a higher flux to the soil C pool than if that additional dead biomass was not present, so S continues to increase after the landslide, and it remains higher than in the base case. Living biomass C density also increases post-landslide, but remains below that of the base case. The decreasing dead biomass C density slightly outpaces the increasing living biomass and soil C densities for the first 122 years following the event, so total C on the deposit decreases over that time by 6 tC ha⁻¹, but then begins to increase again, all while remaining greater than in the base case. Averaged over the entire landslide, the net effect is that B falls behind that of the base case, but D , S , and total C all remain higher than in the base case.

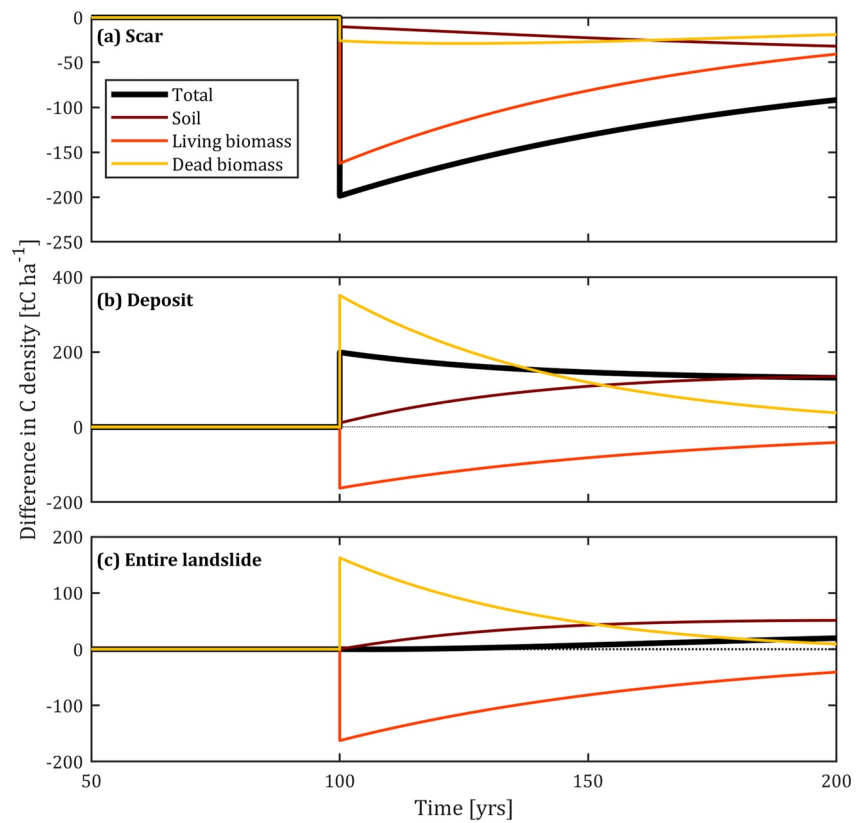


Figure 4. Change in C densities relative to the base case versus time for a single hypothetical landslide at $t = 100$ years in the (a) one-pixel scar, (b) one-pixel deposit, and (c) two-pixel entire extent.

As multiple landslides occur, the effects of single landslides accumulate over time and affect C densities averaged over the entire catchment (Figure 3b). Using the calibrated model parameters (Table 1), living biomass C density falls farther behind that of the base case for about the first 600 years of the model run, after which it remains 0.9 tC ha^{-1} less on average and fluctuates between 0.1 and 2.7 tC ha^{-1} less. Dead biomass C density continues to increase relative to the base case over approximately the first 200 years, then remains 0.3 tC ha^{-1} higher on average, with fluctuations from 0.2 tC ha^{-1} lower to 1.9 tC ha^{-1} higher. Soil C density increases relative to the base case over approximately the first 5,000 years, then averages 3.4 tC ha^{-1} higher while fluctuating between 2.7 and 4.1 tC ha^{-1} higher. Deviations in total C relative to the base case broadly parallel those of soil C, increasing over the first 5,000 years, and then averaging 2.8 tC ha^{-1} higher while fluctuating between 2.3 and 3.5 tC ha^{-1} higher. At the end of each of the additional 100 model runs with imposed random errors, the deviation in total C averaged 2.8 tC ha^{-1} and ranged from 2.0 to 3.9 tC ha^{-1} . The variability among model runs therefore overlapped the variability within a model run, suggesting that the specific magnitude and timing of individual landslide events has a larger impact on deviations in C density than C model parameter uncertainties. Furthermore, all 100 modeled deviations were positive, and they were normally distributed according to the one-sample Kolmogorov-Smirnov test, suggesting that the boost in terrestrial C stocks is robust.

Deviations in average C densities relative to the base case persist even when the model attains a long-term average steady state. This is because the times between landslide events are short relative to the response times of the C pools, especially that of soil C. For example, a cluster of large landslide events occurred from 11,932 to 11,954 years into the model run, which caused catchment-averaged living biomass C to decrease by 1.8 tC ha^{-1} and dead biomass C to increase by 1.5 tC ha^{-1} (Figure 5). With episodic interruptions due to smaller landslide events, those pools then adjusted back toward, but did not attain, their base case values in the subsequent 700 years. The average soil C density was not immediately affected by the landslide cluster, but increased afterward due to the additional input from elevated dead biomass C on landslide deposits and accumulation of new soil C on landslide scars. The rate of soil C accumulation decreased with time following the landslide cluster, and

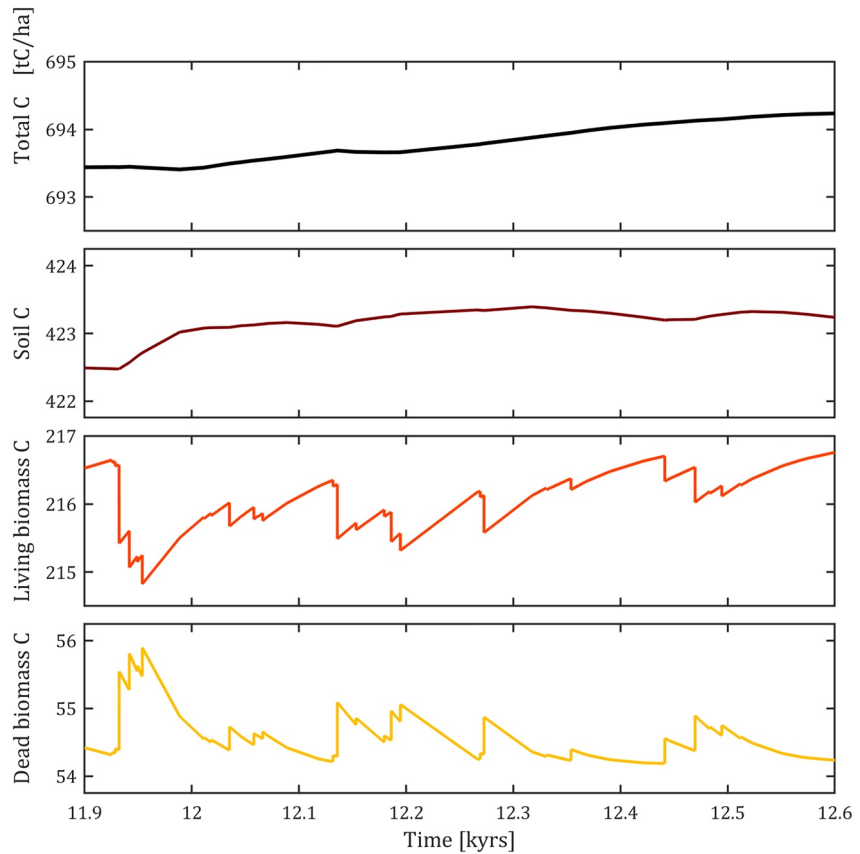


Figure 5. Time-series of mean (a) total, (b) soil, (c) living biomass, and (d) dead biomass C densities near the end of the model run, from 11,900 to 12,600 years.

soil C began to decline slightly by ~ 150 years after the landslide cluster, at 12,089 years. However, a moderate pulse of landslide activity just after that, at 12,136 years, again triggered a subsequent increase in soil C. Total C increased almost monotonically over this period of time, since gains in soil and dead biomass C outweighed losses in living biomass C. In this way, landslides intermittently perturb each of the C pools, maintaining average C densities that differ from those of the base case. C densities deviate most dramatically in the years following relatively large landslide events and trend toward those of the base case during periods of time with relatively low landslide frequency or relatively small landslide events.

Landslides also alter the spatial pattern of C densities and fluxes at a snapshot in time (Figure 6). At the end of the model run, the variances of the dead biomass, soil, and total C pool densities significantly differed from those of the base case, according to the Brown-Forsyth test on absolute deviations from the median. Standard deviation of the dead biomass C density increased from 29.5 to 45.2 tC ha⁻¹, that of soil C increased from 69.1 to 136.2 tC ha⁻¹, and that of total C increased from 179.0 to 219.0 tC ha⁻¹, while that of living biomass C did not significantly differ. The areas of the watershed with C densities most affected by landslides were downslope of the areas with the highest landslide initiation susceptibilities. In particular, the steep south- and west-facing slopes in the northeastern quadrant of the watershed had the highest landslide frequencies, with individual grid cells affected by landslide scars up to 12 times and by deposits up to 11 times in 14,500 years (Figures 6a and 6b). There, and throughout the rest of the watershed, patches of lower than base case C densities developed at higher elevations corresponding to landslide scars, and patches of higher C densities developed on lower elevation footslopes, in low order channels, and along the margins of the Kaasda Héén floodplain, common landslide deposit sites (Figures 6c and 6d). The total area with depressed C densities was 2.2 times greater than the area with elevated C densities, but those elevated C densities outweighed those of the larger area of depressed C densities.

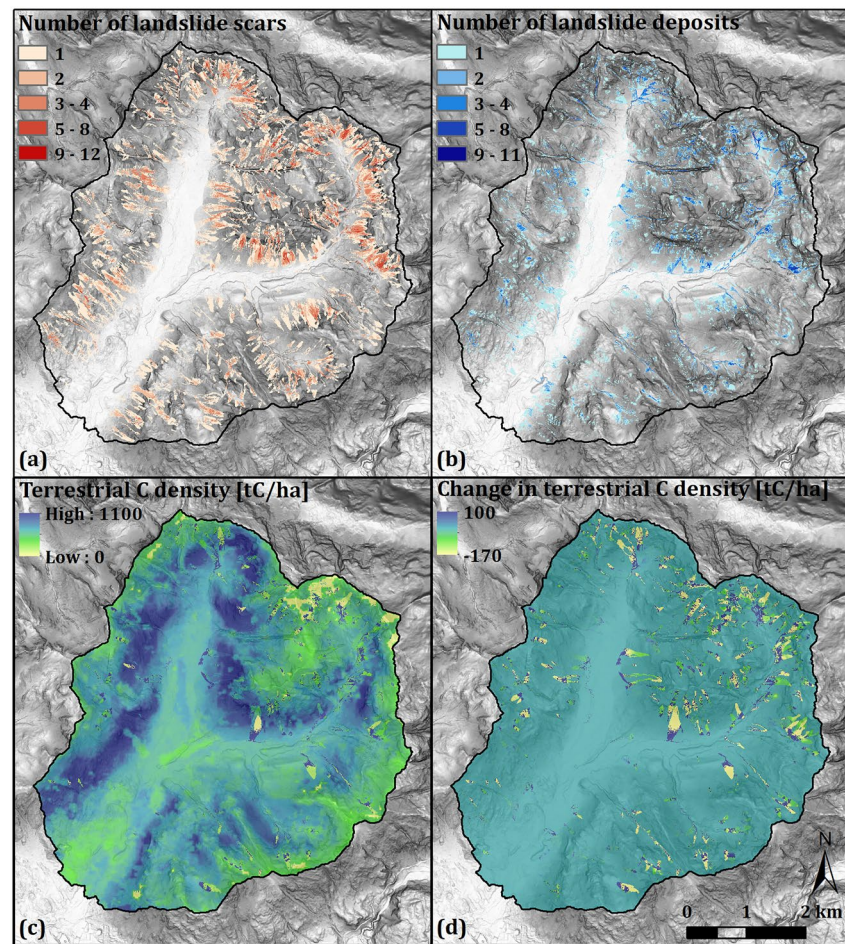


Figure 6. Maps of the number of times each grid cell was affected by a landslide (a) scar or (b) deposit, (c) total terrestrial C density, and (d) its change relative to the base case at the end of the 14,500 yr model run. Background is a lidar-derived slope map. In (c) and (d), color scales saturate at values corresponding to the 97.5th percentile of all pixel values in the watershed.

4.3. Sensitivity of C Density to Landslide Frequency

Historic landslide frequency varies within southeast Alaska, as well as among other mountainous and forested regions throughout the world, which suggests that the effect of landslides on terrestrial C stocks may also vary. Within our study site lidar extent, area-based landslide frequency in a 4 km² moving window ranged from 0 to 6 × 10⁻⁴ yr⁻¹. More broadly, previously documented landslide frequencies at sites where landslide-mobilized C rates have also been determined range from about 10⁻⁵ to 10⁻³ yr⁻¹ (Clark et al., 2016; Hilton et al., 2011; Korup et al., 2019; Ramos Scharrón et al., 2012; Vascik et al., 2021). For the landslide size distribution observed in our study area, this corresponds to a number-based frequency of roughly 10⁻⁴ to 10⁻¹ landslides km⁻² yr⁻¹. We modeled eight additional scenarios in which only landslide frequency was varied over that range to determine the sensitivities of terrestrial C density and response times (Figure 7).

As landslide frequency increases, the fraction of the watershed affected by landslides also increases, such that half the watershed is affected by at least one landslide at a frequency of 1.2 × 10⁻⁴ yr⁻¹, and 78% of the watershed is affected at the greatest frequency simulated, 1.1 × 10⁻³ yr⁻¹ (Figure 7a). Terrestrial C density increases monotonically with landslide frequency, with little increase (<1%) relative to the base case for frequencies less than 10⁻⁵ yr⁻¹, but a larger increase at higher frequencies, attaining a 6.5% increase at the highest simulated landslide frequency (Figure 7b). Increasing landslide frequency also changes response times for each of the C pools, especially for frequencies >10⁻⁴ yr⁻¹ (Figure 7c). The response times of living and dead biomass C are increased by 8% and decreased by 10%, respectively, at the highest landslide frequency, while the response time of soil C is affected more strongly, decreasing by up to 18%. The increase in biomass response time partly counteracts the

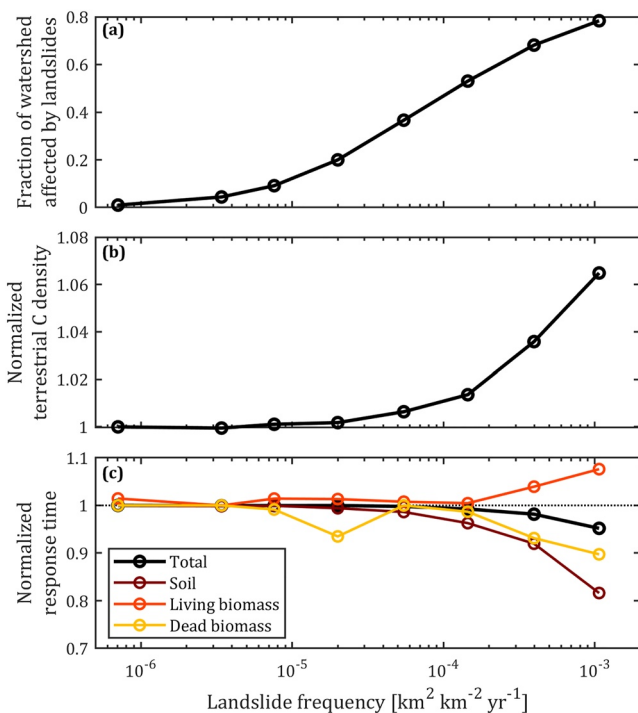


Figure 7. (a) Total fraction of the watershed affected by landslides, (b) normalized average terrestrial C density, and (c) normalized response time versus landslide frequency. Normalized values in (b) and (c) are divided by those of the base case.

decrease in dead biomass and soil response times, so that the response time of total C is decreased by a lower relative amount of up to 5%. Altogether, these results indicate an approximate threshold frequency on the order of 10^{-5} – 10^{-4} yr⁻¹ for landslides to consistently affect terrestrial C dynamics at the study site.

5. Discussion

5.1. Mechanisms for Landslides as C Sources or Sinks

The coupled landslide-terrestrial C model presented in this study implies overall that landslides in southeast Alaska subtly, but systematically, boost C stocks by concentrating C into deposits, creating capacity for new living biomass C to accumulate, and converting living biomass to dead biomass, which subsequently increases soil C density. As such, we consider landslides a C sink because they make the total terrestrial C stocks in a watershed greater at any given time than they would be in the absence of landslides. However, one can more generally define C sources or sinks based on either stocks or fluxes at a given time and location. As a result, scars and deposits, as well the individual C pools, may be considered sources or sinks depending on the specific spatial and temporal scale being analyzed.

On scars, landslides reduce all three C pools to zero, and they subsequently accumulate C as they adjust back toward steady state. This accumulation is a net C flux from the atmosphere to the terrestrial C reservoir, so recent scars could be considered C sinks in terms of the flux, but C sources in terms of the lower amount of total C present there. In the model, no C is retained in the scar, but in reality, soil that is left in the scar may be subject to enhanced decomposition rates, as occurs for surficial soil erosion (Doetterl et al., 2016; Lal, 2019; Van Oost & Six, 2023). However, those rates would have to be

quite high to counter the rate of new C accumulation in our study area. Specifically, new biomass C accumulation rates are initially ~ 3 tC ha⁻¹ yr⁻¹ in our study area, which is higher than typical soil C fluxes of < 1 tC ha⁻¹ yr⁻¹ (Arnalds, 2013; Edwards et al., 2021; Hood et al., 2020; Lilienfein et al., 2003; Oliver et al., 2017; Sollins et al., 1983).

Source or sink behavior of landslide deposits depends on the specific C pool being considered. Biomass behaves as it does on scars and would be considered a sink in terms of the flux, but a source in terms of the stock. On the other hand, landslides elevate both dead biomass and soil C above their steady-state amounts on deposits, which means that loss fluxes from those pools are also elevated. In the model, those loss fluxes can outweigh the accumulation fluxes driven by new biomass growth, so the net flux can be a loss from the deposit. Deposits could therefore be considered local C sources in terms of flux, but local C sinks in terms of the larger total C stock stored there. This study's pool-and-flux model applied to deposits therefore captures the general behavior of enhanced decomposition rates in eroded material, while total C stocks are elevated.

At the watershed scale and over the long term, specifically at times greater than the longest response time for any individual C pool, C accumulation and loss fluxes come into balance as the system approaches steady state. At that time, all individual fluxes are greater than they would be without landslides, but the total net flux averages zero. Therefore, landslides at this scale would not have a source or sink effect in terms of the net flux, but would have a sink effect in terms of the stock. In other words, landslides increase all average C fluxes, which maintains the terrestrial C reservoir at a larger size than if no landslides were occurring.

The fundamental cause of this boost in total C stock is the greater response time of the soil C pool compared to the live biomass C pool. A landslide only redistributes existing C with no immediate effect on total C stocks, so the resulting change in size of each individual pool is what drives subsequent C source or sink behavior. Modeled landslides dramatically increase the amount of dead biomass, which drives an increase in C flux from dead biomass to soil. Once in the soil, that pool's longer response time ensures that the C persists for longer in the landscape than it would otherwise. While it is persisting, other C stocks (all terrestrial C in the scar, as well

as living biomass in the deposit) are also accumulating, increasing total C. For this pattern to be reversed, that is, to make landslides decrease the size of the steady-state terrestrial C reservoir, the response time of the soil C pool would need to be less than that of the live biomass C pool. In that case, landslides would move C to a pool where it would be lost more rapidly than if the landslide had not occurred. In our model, response times are determined by the values of the rate constants, k_i , which have been well constrained with direct measurements for living and dead biomass C (DeMars, 2000; Harmon et al., 2005; Leighty et al., 2006), but inferred based on assumed steady-state reservoir sizes for soil C, likely giving it a larger uncertainty (Equation 4c). Nonetheless, our estimation of the rate constant for soil C loss would need to be biased by about an order of magnitude to make it comparable to that of the live biomass C reservoir, possibly negating the landslide-induced C boost, which is unlikely given the agreement between modeled and independently measured C fluxes (Section 3.2). More generally, soil C response times are likely greater than that of live biomass C in a wide variety of environments (Behre et al., 2005; Lilienfein et al., 2003; Schlesinger, 1990; Wang & Hsieh, 2002), so we suspect our finding that landslides boost total C stocks is applicable beyond our study site and will be robust as more complexity is added to the model.

5.2. Hypothesized Effects of Added Model Complexity

For terrestrial C, a main way to add complexity would be to subdivide the three C pools. If those sub-pools were to have different response times than the three pools included in this study, the effects of landslides on the size and timing of changes to terrestrial C stocks may be different. The biomass reservoirs could be subdivided by size (e.g., stems, branches, or needles), location (e.g., aboveground or belowground), position (e.g., standing or downed), or other characteristics. However, living and dead tree stems make up the vast majority of the biomass C reservoir and have the longest residence times, on the order of decades to centuries (Barrett, 2014; Harmon et al., 2005; Leighty et al., 2006), so they should dominate evolution of the biomass reservoir as a whole over the long term, as in our three-pool model. On the other hand, residence times of C in soil can vary as a function of depth, wetness, and especially whether it is mineral associated C (MAC), all of which could be used to subdivide the soil C reservoir (Oades, 1988). In particular, MAC is typically the largest constituent of soil C (Georgiou et al., 2022) and has much longer residence times than other constituents, so distinguishing that pool would likely lengthen the response time of the system as a whole. We therefore hypothesize that explicitly modeling the MAC pool would make the landslide-induced boost in soil C more persistent over time and increase the long-term average size of the soil C reservoir more than predicted by our single soil C pool model.

An additional element of model complexity that may have an outsized influence on results is the shape of the living biomass C accumulation curve. In our model, living biomass C density monotonically increases, but there is evidence that biomass C actually peaks on the order of hundreds of years after disturbance before retrogressing to its long-term, steady-state value over thousands of years, both in our study region (DeMars, 2000; Leighty et al., 2006) and more generally (Wardle et al., 2004). Landslides may contribute to that peak by delivering nutrients from scars to deposits or by disrupting soil structures that inhibit biomass growth throughout their runoff path. Landslides could therefore increase living biomass C stocks if they occurred frequently enough to keep portions of the landscape near the peak of the biomass accumulation curve. This effect would most likely be strongest at deposition sites where debris flows inundate standing forests without necessarily killing all the trees. In our Kaasda Héen study area, modeled landslide recurrence intervals at any point in the landscape are likely too long ($\geq 1,200$ years) for that effect to be important, since biomass C densities would have time to return to steady-state between landslide events, but it could be important in areas with higher landslide frequencies.

Furthermore, the steady-state C densities assumed in our model (Equation 4) may themselves be shifting with time, which could be incorporated in the model by allowing the parameters k_i to vary with time. Steady-state C density at any moment in time, which is determined from k_i in Equation 4 at that time, is termed the C storage capacity, and modeled C densities move toward that capacity, absent disturbance (Luo et al., 2015, 2017). If a reservoir's response time is short relative to the timescale of its changing storage capacity, actual C density should closely track C storage capacity over time. But, if capacity changes quickly relative to response time, actual C densities will lag the current C storage capacity. Our model provides a first order estimate of the relevant response times for southeast Alaska, suggesting that soil C requires on the order of 1,000 years to adjust to a change in C storage capacity, while living and dead biomass both require on the order of 100 years. The purpose of this study was to characterize the general, long-term effects of landslides on terrestrial C stocks, but more specific

and short-term predictions involving other natural or human-caused disturbances could also be simulated by incorporating time-varying parameters.

In southeast Alaska, total living biomass C storage capacity has increased by an average of $0.12 \text{ tC ha}^{-1} \text{ yr}^{-1}$ over recent decades (Buma & Barrett, 2015; assuming biomass is 50% C), a fraction of our modeled $1.0 \text{ tC ha}^{-1} \text{ yr}^{-1}$ steady-state flux (Table 1). Although most of these gains occurred to the north of our study area, they suggest regionally that C storage capacity likely exceeds current C density, and the pattern of ongoing C change has implications for landslide-terrestrial C interactions. Gains in forest area were concentrated around tree line ($\sim 500 \text{ m AMSL}$), overlapping typical landslide scar locations, while gains in biomass density were concentrated at lower elevations ($< 350 \text{ m AMSL}$) and slopes ($< 20^\circ$), which are common landslide deposit sites (Figures 1 and 6). These patterns and our modeling suggest that landslides will mobilize more living biomass C than in the past, which will subsequently elevate dead biomass, soil, and total C densities, all else being equal. Predicted increases in landslide frequency due to increased precipitation extremes would compound that effect (Crozier, 2010; Gariano & Guzzetti, 2016; Shanley et al., 2015). However, rates of change of dead biomass and soil C stocks have not been determined for the region and are needed for a more complete understanding of how climate change is currently affecting the trajectory of total terrestrial C.

For the landslide component of our model, the available landslide inventory provided data to simulate 2D plan-form landslide geometries on static topography, such that soil depths along with landslide initiation points, sizes, runout paths, and deposit extents did not depend on previous landslides. The 2D assumption means that soil depth is not explicitly resolved, but it is implicitly assumed to be capable of containing the modeled C density at any time and to have no direct influence on the rate constants, k_i , that determine soil C fluxes (Figure 2, Equation 3). In landslide scars that expose bedrock, the time required to accumulate new sediments may limit subsequent C accumulation rates, thereby reducing the size of the terrestrial C boost predicted by our model. However, in landslide deposits the model currently does not account for the smaller rate constants (i.e., longer turnover times) associated with deeper C burial, and doing so would likely increase the predicted terrestrial C boost. The assumption of static topography means that landslide runout and deposition is not influenced by previous runout paths or deposits. In reality, erosion during runout would likely cause future landslides to follow similar paths in increasingly confined channels, which are present in the study area (Patton et al., 2022), while existing deposits would tend to divert future landslide deposition to nearby lower elevation areas. This would likely reduce the area with depressed C densities affected by landslide scars, but increase the area with elevated C densities affected by landslide deposits. Overall, the net effect of adding complexity to the landslide component of the model is unclear with respect to total terrestrial C stocks, but it is probably minimal in our study watershed since landslide recurrence intervals are generally long (1,200 to $> 14,500$ years) compared to timescales for soil production and transport in temperate rainforests (e.g., Heimsath et al., 2001). Furthermore, none of these model improvements should counteract the fundamental behavior that landslides only redistribute existing terrestrial C, and all C pools subsequently either increase monotonically, or decrease while remaining elevated with respect to the base case.

5.3. Landslides and the Global C Cycle

As shown by our model, landslides likely boost terrestrial C stocks in southeast Alaska, but whether they are more broadly a net C source or sink with respect to the atmosphere globally over geologic time remains uncertain. Explicitly considering the pathways included in the generalized loss fluxes of our terrestrial C model (F_{DL} and F_{SL}) can shed light on this question. Those fluxes include transfer of terrestrial C to the atmosphere through microbial respiration and decomposition, as well as transport of DOC and POC through rivers to marine settings. Of those fluxes, POC export and burial in marine sediments sequesters C for much longer periods of time than the millennial turnover times of soil C (Berner, 1982; Blair & Aller, 2012; Hedges & Keil, 1995; Hedges et al., 1997). Since our model is calibrated to account for that loss of terrestrial C, its preservation in marine sediments represents an additional landslide-induced C sink. Burial rates of terrestrial POC in southeast Alaskan fjord sediments are globally high, suggesting they are important C sinks during interglacial times, and possibly longer if those POC-rich sediments are subsequently transported to and buried on the continental shelf (Cui et al., 2016; Smith et al., 2015). Another important way landslides affect C fluxes outside the terrestrial C system is by exposing fresh bedrock and increasing weathering rates. Oxidative weathering releases C to the atmosphere in some areas with sedimentary rocks, but silicate weathering consumes a similar amount of C over geologic timescales, so the net effect of weathering on C sequestration from the atmosphere is unclear (Hilton & West, 2020). Overall, we

infer that landslides are globally most likely a net C sink over a wide range of timescales because they (a) boost terrestrial C stocks, as shown by our model, (b) facilitate burial of C in marine sediments, and (c) cause comparable increases of weathering rates in different rock types.

To further place the importance of landslides to boosting terrestrial C stocks in a global context, we make a rough order of magnitude estimate of the plausible absolute increase in terrestrial C over landslide-prone regions of the world. To identify landslide-prone regions, we threshold the World Bank's global landslide hazard map at a qualitative threshold of "low," which roughly corresponds to a frequency exceeding 10^{-4} landslides $\text{km}^{-2} \text{yr}^{-2}$, including both rainfall and earthquake-triggered landslides (Redshaw & Bottomley, 2020). We then extract total biomass and soil C to 30 cm depth within that landslide-prone region from the global models of Spawn and Gibbs (2020) and SoilGrids 2.0 (Poggio et al., 2021), respectively. According to those data sets, landslide-prone regions cover 36 million km^2 of Earth's surface and contain 358 GtC in biomass and the upper 30 cm of soil. This is $\sim 28\%$ of the earth's ice-free land area, but $\sim 37\%$ of the total soil and biomass C, indicating that landslides tend to occur in regions with larger than average terrestrial C densities, especially forested and mountainous regions. If those forested regions have a similar difference in biomass and soil C response times, our model result that landslides boost terrestrial C stocks should generally apply. Calibrated to our study site, historic rates of landsliding boost C stocks by a fraction of a percent to several percent. Although small as a percentage, this suggests the global terrestrial C reservoir is plausibly of order $\sim 10^0\text{--}10^2$ GtC larger than it would be in the absence of landslides. For context, this is likely more than the terrestrial C currently stored in all of southeast Alaska (Leighty et al., 2006).

6. Conclusions

We coupled a pool-and-flux model for the terrestrial C cycle with a stochastic landslide model to determine the effect of landslide-driven movement of C across the landscape on the size of the terrestrial C reservoir in forested southeast Alaska. In the absence of landslides, the living biomass, dead biomass, and soil C pools have mean steady-state densities of 217, 54, and 427 tC ha^{-1} , respectively, in the Kaasda Héen (Indian River) watershed study site near Sitka. Relative to that base case, introducing landslides with the observed size distribution and frequency of 4×10^{-3} landslides $\text{km}^{-2} \text{yr}^{-1}$ decreases long-term average living biomass C by $\sim 0.4\%$, increases dead biomass C by $\sim 0.6\%$, and increases soil C by $\sim 0.8\%$, resulting in a net increase in total terrestrial C of $\sim 0.4\%$. Landslides cause these subtle, but systematic, changes by episodically redistributing terrestrial C from scars to deposits and converting living biomass C to dead biomass C. This redistribution elevates soil C stocks in deposits, which have a longer response time than biomass, preserving C in the landscape for longer than if no landslides occurred. Post-landslide, C densities either increase monotonically or decrease toward, but remain greater than, their base case densities, so long as the time between landslides is short compared to the response times of the C pools. Simulating a range of plausible landslide frequencies indicates that this landslide-induced boost in C density becomes important ($>1\%$) at a frequency on the order of 10^{-4}yr^{-1} and increases nonlinearly to reach 6.5% by a frequency of 10^{-3}yr^{-1} . Since soil C response times are generally longer than those of biomass C, we expect that this boost also occurs in other forested and landslide-prone regions of the globe. Since landslides also facilitate offshore burial of terrestrial C, we infer that landslides generally are likely a net C sink with respect to the atmosphere over a wide range of time scales. If increasing precipitation extremes due to global climate change cause an increase in landslide frequency, landslides are likely to act as a natural buffer against further increasing atmospheric CO_2 levels.

Data Availability Statement

Lidar data are available from the Alaska Division of Geological & Geophysical Surveys (Daanen et al., 2020), and the landslide inventory is available through the U. S. Department of Agriculture Ag Data Commons (U. S. Department of Agriculture Forest Service, 2018). All data and code related to southeast Alaska biomass and soil C maps have been previously published and made publicly available (Buma & Thompson, 2019; McNicol et al., 2019). Code for the model presented in this study is included in Supporting Information S1. Global landslide frequency maps are available through the World Bank Data Catalog (Redshaw & Bottomley, 2020), biomass C maps are available through Oak Ridge National Laboratory Distributed Active Archive Center for Biogeochemical Dynamics (Spawn & Gibbs, 2020), and soil C maps are available through the World Soil Information Service (Poggio et al., 2021).

Acknowledgments

This work was funded by NSF-1711986 (Booth) and NSF-1711974 (Buma and Nagorski), and benefitted from discussions at the 2019 European Geosciences Union Galileo Conference: Perturbations to Earth Surface Dynamics Caused by Extreme Events, supported partly by NSF-1924710. This manuscript has been made open access through support provided by Portland State University Library.

References

- Arnalds, O. (2013). The influence of volcanic tephra (ash) on ecosystems. *Advances in Agronomy*, *121*, 331–380.
- Barrett, T. (2014). *Storage and flux of carbon in live trees, snags, and logs in the Chugach and Tongass National Forests*. General technical reports PNW-GTR-889 (Vol. 44, p. 889). US Department of Agriculture, Forest Service, Pacific Northwest Research Station.
- Begét, J. E., & Motyka, R. J. (1998). New dates on late Pleistocene dacitic tephra from the Mount Edgecumbe volcanic field, southeastern Alaska. *Quaternary Research*, *49*(1), 123–125. <https://doi.org/10.1006/qres.1997.1945>
- Berhe, A. A., Harden, J. W., Harte, J., & Torn, M. S. (2005). *Soil degradation and global change: Role of soil erosion and deposition in carbon sequestration*. University of California International and Area Studies.
- Berhe, A. A., Harden, J. W., Torn, M. S., & Harte, J. (2008). Linking soil organic matter dynamics and erosion-induced terrestrial carbon sequestration at different landform positions. *Journal of Geophysical Research*, *113*(G4). <https://doi.org/10.1029/2008JG000751>
- Berhe, A. A., Harden, J. W., Torn, M. S., Kleber, M., Burton, S. D., & Harte, J. (2012). Persistence of soil organic matter in eroding versus depositional landform positions. *Journal of Geophysical Research*, *117*(G2). <https://doi.org/10.1029/2011JG001790>
- Berhe, A. A., Harte, J., Harden, J. W., & Torn, M. S. (2007). The significance of the erosion-induced terrestrial carbon sink. *BioScience*, *57*(4), 337–346. <https://doi.org/10.1641/b570408>
- Berner, R. A. (1982). Burial of organic carbon and pyrite sulfur in the modern ocean: Its geochemical and environmental significance. *American Journal of Science*, *282*(4), 451–473. <https://doi.org/10.2475/ajs.282.4.451>
- Berti, M., & Simoni, A. (2007). Prediction of debris flow inundation areas using empirical mobility relationships. *Geomorphology*, *90*(1–2), 144–161. <https://doi.org/10.1016/j.geomorph.2007.01.014>
- Berti, M., & Simoni, A. (2014). DFLOWZ: A free program to evaluate the area potentially inundated by a debris flow. *Computers & Geosciences*, *67*, 14–23. <https://doi.org/10.1016/j.cageo.2014.02.002>
- Bianchi, T. S., Cui, X., Blair, N. E., Burdige, D. J., Eglinton, T. I., & Galy, V. (2018). Centers of organic carbon burial and oxidation at the land-ocean interface. *Organic Geochemistry*, *115*, 138–155. <https://doi.org/10.1016/j.orggeochem.2017.09.008>
- Billings, S. A., Richter, D. D. B., Ziegler, S. E., Prestegard, K., & Wade, A. M. (2019). Distinct contributions of eroding and depositional profiles to land-atmosphere CO₂ exchange in two contrasting forests. *Frontiers in Earth Science*, *7*. Article 36. <https://doi.org/10.3389/feart.2019.00036>
- Blair, N. E., & Aller, R. C. (2012). The fate of terrestrial organic carbon in the marine environment. *Annual Review of Marine Science*, *4*(1), 401–423. <https://doi.org/10.1146/annurev-marine-120709-142717>
- Booth, A. M., Roering, J. J., & Perron, J. T. (2009). Automated landslide mapping using spectral analysis and high-resolution topographic data: Puget Sound lowlands, Washington, and Portland Hills, Oregon. *Geomorphology*, *109*(3–4), 132–147. <https://doi.org/10.1016/j.geomorph.2009.02.027>
- Booth, A. M., Sifford, C., Vascik, B., Siebert, C., & Buma, B. (2020). Large wood inhibits debris flow runoff in forested southeast Alaska. *Earth Surface Processes and Landforms*, *45*(7), 1555–1568. <https://doi.org/10.1002/esp.4830>
- Bufe, A., Hovius, N., Emberson, R., Rugenstein, J. K., Galy, A., Hassenruck-Gudipati, H. J., & Chang, J. M. (2021). Co-variation of silicate, carbonate and sulfide weathering drives CO₂ release with erosion. *Nature Geoscience*, *14*(4), 211–216. <https://doi.org/10.1038/s41561-021-00714-3>
- Buma, B., & Barrett, T. M. (2015). Spatial and topographic trends in forest expansion and biomass change, from regional to local scales. *Global Change Biology*, *21*(9), 3445–3454. <https://doi.org/10.1111/gcb.12915>
- Buma, B., & Johnson, A. C. (2015). The role of windstorm exposure and yellow cedar decline on landslide susceptibility in southeast Alaskan temperate rainforests. *Geomorphology*, *228*, 504–511. <https://doi.org/10.1016/j.geomorph.2014.10.014>
- Buma, B., Krapek, J., & Edwards, R. T. (2016). Watershed-scale forest biomass distribution in a perhumid temperate rainforest as driven by topographic, soil, and disturbance variables. *Canadian Journal of Forest Research*, *46*(6), 844–854. <https://doi.org/10.1139/cjfr-2016-0041>
- Buma, B., & Thompson, T. (2019). Long-term exposure to more frequent disturbances increases baseline carbon in some ecosystems: Mapping and quantifying the disturbance frequency-ecosystem C relationship. [Dataset]. PLoS One, *14*(2), e0212526. <https://doi.org/10.1371/journal.pone.0212526>
- Carrara, A., Cardinali, M., & Guzzetti, F. (1992). Uncertainty in assessing landslide hazard and risk. *ITC Journal*, *(2)*, 172–183.
- Clark, K. E., West, A. J., Hilton, R. G., Asner, G. P., Quesada, C. A., Silman, M. R., et al. (2016). Storm-triggered landslides in the Peruvian Andes and implications for topography, carbon cycles, and biodiversity. *Earth Surface Dynamics*, *4*(1), 47–70. <https://doi.org/10.5194/esurf-4-47-2016>
- Croissant, T., Hilton, R. G., Li, G. K., Howarth, J., Wang, J., Harvey, E. L., et al. (2021). Pulsed carbon export from mountains by earthquake-triggered landslides explored in a reduced-complexity model. *Earth Surface Dynamics*, *9*(4), 823–844. <https://doi.org/10.5194/esurf-9-823-2021>
- Crozier, M. J. (2010). Deciphering the effect of climate change on landslide activity: A review. *Geomorphology*, *124*(3–4), 260–267. <https://doi.org/10.1016/j.geomorph.2010.04.009>
- Cui, X., Bianchi, T. S., Savage, C., & Smith, R. W. (2016). Organic carbon burial in fjords: Terrestrial versus marine inputs. *Earth and Planetary Science Letters*, *451*, 41–50. <https://doi.org/10.1016/j.epsl.2016.07.003>
- Daanen, R. P., Wolken, G. J., & Herbst, A. M. (2020). Lidar-derived elevation data for Sitka, Alaska. [Dataset]. Alaska Division of Geological & Geophysical Surveys. Raw data file 2020-13. <https://doi.org/10.14509/30531>
- DeMars, D. J. (2000). *Stand-density study of spruce-hemlock stands in southeastern Alaska*. General technical report PNW-GTR-496 (Vol. 60, p. 496). US Department of Agriculture, Forest Service, Pacific Northwest Research Station.
- Dialynas, Y. G., Bastola, S., Bras, R. L., Marin-Spiotta, E., Silver, W. L., Arnone, E., & Noto, L. V. (2016). Impact of hydrologically driven hillslope erosion and landslide occurrence on soil organic carbon dynamics in tropical watersheds. *Water Resources Research*, *52*(11), 8895–8919. <https://doi.org/10.1002/2016WR018925>
- Dietrich, W. E., Bellugi, D. G., Sklar, L. S., Stock, J. D., Heimsath, A. M., & Roering, J. J. (2003). Geomorphic transport laws for predicting landscape form and dynamics. *Geophysical Monograph-American Geophysical Union*, *135*, 103–132. <https://doi.org/10.1029/135GM09>
- Doetterl, S., Berhe, A. A., Nadeu, E., Wang, Z., Sommer, M., & Fiener, P. (2016). Erosion, deposition and soil carbon: A review of process-level controls, experimental tools and models to address C cycling in dynamic landscapes. *Earth-Science Reviews*, *154*, 102–122. <https://doi.org/10.1016/j.earscirev.2015.12.005>
- Doetterl, S., Six, J., Van Wesemael, B., & Van Oost, K. (2012). Carbon cycling in eroding landscapes: Geomorphic controls on soil organic C pool composition and C stabilization. *Global Change Biology*, *18*(7), 2218–2232. <https://doi.org/10.1111/j.1365-2486.2012.02680.x>
- Edwards, R. T., D'Amore, D. V., Biles, F. E., Fellman, J. B., Hood, E. W., Trubilowicz, J. W., & Floyd, W. C. (2021). Riverine dissolved organic carbon and freshwater export in the eastern Gulf of Alaska. *Journal of Geophysical Research: Biogeosciences*, *126*(1), e2020JG005725. <https://doi.org/10.1029/2020JG005725>

- Emberson, R., Galy, A., & Hovius, N. (2018). Weathering of reactive mineral phases in landslides acts as a source of carbon dioxide in mountain belts. *Journal of Geophysical Research: Earth Surface*, *123*(10), 2695–2713. <https://doi.org/10.1029/2018JF004672>
- Emberson, R., Hovius, N., Galy, A., & Marc, O. (2016). Oxidation of sulfides and rapid weathering in recent landslides. *Earth Surface Dynamics*, *4*(3), 727–742. <https://doi.org/10.5194/esurf-4-727-2016>
- Freeman, T. G. (1991). Calculating catchment area with divergent flow based on a regular grid. *Computers & Geosciences*, *17*(3), 413–422. [https://doi.org/10.1016/0098-3004\(91\)90048-i](https://doi.org/10.1016/0098-3004(91)90048-i)
- Frith, N. V., Hilton, R. G., Howarth, J. D., Gröcke, D. R., Fitzsimons, S. J., Croissant, T., et al. (2018). Carbon export from mountain forests enhanced by earthquake-triggered landslides over millennia. *Nature Geoscience*, *11*(10), 772–776. <https://doi.org/10.1038/s41561-018-0216-3>
- Galy, V., France-Lanord, C., Beyssac, O., Faure, P., Kudrass, H., & Palhol, F. (2007). Efficient organic carbon burial in the Bengal fan sustained by the Himalayan erosional system. *Nature*, *450*(7168), 407–410. <https://doi.org/10.1038/nature06273>
- Gariano, S. L., & Guzzetti, F. (2016). Landslides in a changing climate. *Earth-Science Reviews*, *162*, 227–252. <https://doi.org/10.1016/j.earscirev.2016.08.011>
- Gavin, D. G., Brubaker, L. B., & Lertzman, K. P. (2003). Holocene fire history of a coastal temperate rain forest based on soil charcoal radiocarbon dates. *Ecology*, *84*(1), 186–201. [https://doi.org/10.1890/0012-9658\(2003\)084\[0186:hfoac\]2.0.co;2](https://doi.org/10.1890/0012-9658(2003)084[0186:hfoac]2.0.co;2)
- Gehrels, G. E., & Berg, H. C. (1992). *Geologic map of Southeastern Alaska*. US Geological Survey Open-File Report 84-886. US Geological Survey.
- Georgiou, K., Jackson, R. B., Vindušková, O., Abramoff, R. Z., Ahlström, A., Feng, W., et al. (2022). Global stocks and capacity of mineral-associated soil organic carbon. *Nature Communications*, *13*(1), 1–12. <https://doi.org/10.1038/s41467-022-31540-9>
- Gomi, T., Sidle, R. C., & Swanston, D. N. (2004). Hydrogeomorphic linkages of sediment transport in headwater streams, Maybeso experimental forest, southeast Alaska. *Hydrological Processes*, *18*(4), 667–683. <https://doi.org/10.1002/hyp.1366>
- Guthrie, R. H., & Evans, S. G. (2004). Analysis of landslide frequencies and characteristics in a natural system, coastal British Columbia. *Earth Surface Processes and Landforms*, *29*(11), 1321–1339. <https://doi.org/10.1002/esp.1095>
- Hansen, B. C., & Engstrom, D. R. (1996). Vegetation history of Pleasant Island, southeastern Alaska, since 13,000 yr BP. *Quaternary Research*, *46*(2), 161–175. <https://doi.org/10.1006/qres.1996.0056>
- Harmon, M., Fath, B., Yatskov, M., Sexton, J., & Trummer, L. (2005). The fate of dead spruce on the Kenai Peninsula: A preliminary report. USDA Forest Service Technical Report R10-TP-134.
- Hedges, J. I., & Keil, R. G. (1995). Sedimentary organic matter preservation: An assessment and speculative synthesis. *Marine Chemistry*, *49*(2–3), 81–115. [https://doi.org/10.1016/0304-4203\(95\)00013-h](https://doi.org/10.1016/0304-4203(95)00013-h)
- Hedges, J. I., Keil, R. G., & Benner, R. (1997). What happens to terrestrial organic matter in the ocean? *Organic Geochemistry*, *27*(5–6), 195–212. [https://doi.org/10.1016/s0146-6380\(97\)00066-1](https://doi.org/10.1016/s0146-6380(97)00066-1)
- Heimsath, A. M., Dietrich, W. E., Nishiizumi, K., & Finkel, R. C. (2001). Stochastic processes of soil production and transport: Erosion rates, topographic variation and cosmogenic nuclides in the Oregon Coast Range. *Earth Surface Processes and Landforms*, *26*(5), 531–552. <https://doi.org/10.1002/esp.209>
- Hilton, R. G. (2017). Climate regulates the erosional carbon export from the terrestrial biosphere. *Geomorphology*, *277*, 118–132. <https://doi.org/10.1016/j.geomorph.2016.03.028>
- Hilton, R. G., Galy, A., & Hovius, N. (2008). Riverine particulate organic carbon from an active mountain belt: Importance of landslides. *Global Biogeochemical Cycles*, *22*(1). <https://doi.org/10.1029/2006gb002905>
- Hilton, R. G., Galy, A., Hovius, N., Chen, M. C., Horng, M. J., & Chen, H. (2008). Tropical-cyclone-driven erosion of the terrestrial biosphere from mountains. *Nature Geoscience*, *1*(11), 759–762. <https://doi.org/10.1038/ngeo333>
- Hilton, R. G., Meunier, P., Hovius, N., Bellingham, P. J., & Galy, A. (2011). Landslide impact on organic carbon cycling in a temperate montane forest. *Earth Surface Processes and Landforms*, *36*(12), 1670–1679. <https://doi.org/10.1002/esp.2191>
- Hilton, R. G., & West, A. J. (2020). Mountains, erosion and the carbon cycle. *Nature Reviews Earth & Environment*, *1*(6), 284–299. <https://doi.org/10.1038/s43017-020-0058-6>
- Hood, E., Fellman, J. B., & Spencer, R. G. (2020). Glacier loss impacts riverine organic carbon transport to the ocean. *Geophysical Research Letters*, *47*(19), e2020GL089804. <https://doi.org/10.1029/2020GL089804>
- Houghton, J. T., Jenkins, G. J., & Ephraums, J. J. (1990). Climate change: The IPCC scientific assessment. *American Scientist*, *80*(6).
- Iverson, R. M., Schilling, S. P., & Vallance, J. W. (1998). Objective delineation of lahar-inundation hazard zones. *Geological Society of America Bulletin*, *110*(8), 972–984. [https://doi.org/10.1130/0016-7606\(1998\)110<0972:odolih>2.3.co;2](https://doi.org/10.1130/0016-7606(1998)110<0972:odolih>2.3.co;2)
- Johnson, A. C., Swanston, D. N., & McGee, K. E. (2000). Landslide initiation, runoff, and deposition within clearcuts and old-growth forests of Alaska. *JAWRA Journal of the American Water Resources Association*, *36*(1), 17–30. <https://doi.org/10.1111/j.1752-1688.2000.tb04245.x>
- Karl, S. M., Haessler, P. J., Himmelberg, G. R., Zumsteg, C. L., Layer, P. W., Friedman, R. M., et al. (2015). Geologic map of Baranof Island, southeastern Alaska (U.S. Geological Survey Scientific Investigations Map 3335, 82 p., 1 sheet). <https://doi.org/10.3133/sim335>
- Korup, O., Seidemann, J., & Mohr, C. H. (2019). Increased landslide activity on forested hillslopes following two recent volcanic eruptions in Chile. *Nature Geoscience*, *12*(4), 284–289. <https://doi.org/10.1038/s41561-019-0315-9>
- Lal, R. (2019). Accelerated soil erosion as a source of atmospheric CO₂. *Soil and Tillage Research*, *188*, 35–40. <https://doi.org/10.1016/j.still.2018.02.001>
- Lancaster, S. T., Hayes, S. K., & Grant, G. E. (2003). Effects of wood on debris flow runoff in small mountain watersheds. *Water Resources Research*, *39*(6). <https://doi.org/10.1029/2001WR001227>
- Leighty, W. W., Hamburg, S. P., & Caouette, J. (2006). Effects of management on carbon sequestration in forest biomass in southeast Alaska. *Ecosystems*, *9*(7), 1051–1065. <https://doi.org/10.1007/s10021-005-0028-3>
- Lilienfein, J., Qualls, R. G., Uselman, S. M., & Bridgman, S. D. (2003). Soil formation and organic matter accretion in a young andesitic chronosequence at Mt. Shasta, California. *Geoderma*, *116*(3–4), 249–264. [https://doi.org/10.1016/s0167-7061\(03\)00086-7](https://doi.org/10.1016/s0167-7061(03)00086-7)
- Luo, Y., Keenan, T. F., & Smith, M. (2015). Predictability of the terrestrial carbon cycle. *Global Change Biology*, *21*(5), 1737–1751. <https://doi.org/10.1111/gcb.12766>
- Luo, Y., Shi, Z., Lu, X., Xia, J., Liang, J., Jiang, J., et al. (2017). Transient dynamics of terrestrial carbon storage: Mathematical foundation and its applications. *Biogeosciences*, *14*(1), 145–161. <https://doi.org/10.5194/bg-14-145-2017>
- Malamud, B. D., Turcotte, D. L., Guzzetti, F., & Reichenbach, P. (2004). Landslide inventories and their statistical properties. *Earth Surface Processes and Landforms*, *29*(6), 687–711. <https://doi.org/10.1002/esp.1064>
- Manzoni, S., & Porporato, A. (2009). Soil carbon and nitrogen mineralization: Theory and models across scales. *Soil Biology and Biochemistry*, *41*(7), 1355–1379. <https://doi.org/10.1016/j.soilbio.2009.02.031>

- Martin, Y., Rood, K., Schwab, J. W., & Church, M. (2002). Sediment transfer by shallow landsliding in the Queen Charlotte Islands, British Columbia. *Canadian Journal of Earth Sciences*, *39*(2), 189–205. <https://doi.org/10.1139/e01-068>
- McDougall, S. (2017). 2014 Canadian Geotechnical Colloquium: Landslide runoff analysis—Current practice and challenges. *Canadian Geotechnical Journal*, *54*(5), 605–620. <https://doi.org/10.1139/cgj-2016-0104>
- McNicol, G., Bulmer, C., D'Amore, D., Sanborn, P., Saunders, S., Giesbrecht, I., et al. (2019). Large, climate-sensitive soil carbon stocks mapped with pedology-informed machine learning in the North Pacific coastal temperate rainforest. [Dataset]. *Environmental Research Letters*, *14*(1), 014004. <https://doi.org/10.1088/1748-9326/aad52>
- Mudd, S. M., & Yoo, K. (2010). Reservoir theory for studying the geochemical evolution of soils. *Journal of Geophysical Research*, *115*(F3), F03030. <https://doi.org/10.1029/2009JF001591>
- Oades, J. M. (1988). The retention of organic matter in soils. *Biogeochemistry*, *5*(1), 35–70. <https://doi.org/10.1007/bf02180317>
- Oliver, A. A., Tank, S. E., Giesbrecht, I., Korver, M. C., Floyd, W. C., Sanborn, P., et al. (2017). A global hotspot for dissolved organic carbon in hypermaritime watersheds of coastal British Columbia. *Biogeosciences*, *14*(15), 3743–3762. <https://doi.org/10.5194/bg-14-3743-2017>
- Patton, A. I., Roering, J. J., & Orland, E. (2022). Debris flow initiation in postglacial terrain: Insights from shallow landslide initiation models and geomorphic mapping in Southeast Alaska. *Earth Surface Processes and Landforms*, *47*(6), 1583–1598. <https://doi.org/10.1002/esp.5336>
- Poggio, L., De Sousa, L. M., Batjes, N. H., Heuvelink, G., Kempen, B., Ribeiro, E., & Rossiter, D. (2021). SoilGrids 2.0: Producing soil information for the globe with quantified spatial uncertainty. [Dataset]. *Soil*, *7*(1), 217–240. <https://doi.org/10.5194/soil-7-217-2021>
- Praetorius, S., Mix, A., Jensen, B., Froese, D., Milne, G., Wolhowe, M., et al. (2016). Interaction between climate, volcanism, and isostatic rebound in Southeast Alaska during the last deglaciation. *Earth and Planetary Science Letters*, *452*, 79–89. <https://doi.org/10.1016/j.epsl.2016.07.033>
- Ramos Scharrón, C. E., Castellanos, E. J., & Restrepo, C. (2012). The transfer of modern organic carbon by landslide activity in tropical montane ecosystems. *Journal of Geophysical Research*, *117*(G3). <https://doi.org/10.1029/2011JG001838>
- Ran, L., Lu, X. X., & Xin, Z. (2014). Erosion-induced massive organic carbon burial and carbon emission in the Yellow River basin, China. *Biogeosciences*, *11*(4), 945–959. <https://doi.org/10.5194/bg-11-945-2014>
- Redshaw, P., & Bottomley, J. (2020). The global landslide hazard map [Dataset]. The World Bank, Final project report, Job number 271785-00. Retrieved from <https://datacatalog.worldbank.org/search/dataset/0037584>
- Richardson, P., & Karlstrom, L. (2019). The multi-scale influence of topography on lava flow morphology. *Bulletin of Volcanology*, *81*(4), 1–17. <https://doi.org/10.1007/s00445-019-1278-9>
- Rickenmann, D. (1999). Empirical relationships for debris flows. *Natural Hazards*, *19*(1), 47–77. <https://doi.org/10.1023/a:1008064220727>
- Riehle, J. R. (1996). *The Mount Edgecumbe volcanic field: A geologic history* (Vol. 114). US Department of Agriculture, Forest Service.
- Riehle, J. R., Brew, D. A., Reed, K. M., & Bartsch-Winkler, S. (1984). Explosive latest Pleistocene (?) and Holocene activity of the mount Edgecumbe volcanic field, Alaska. *US Geological Survey Circular*, *939*, 111–114.
- Rosenbloom, N. A., Doney, S. C., & Schimel, D. S. (2001). Geomorphic evolution of soil texture and organic matter in eroding landscapes. *Global Biogeochemical Cycles*, *15*(2), 365–381. <https://doi.org/10.1029/1999gb001251>
- Rosenbloom, N. A., Harden, J. W., Neff, J. C., & Schimel, D. S. (2006). Geomorphic control of landscape carbon accumulation. *Journal of Geophysical Research*, *111*(G1), G01004. <https://doi.org/10.1029/2005JG000077>
- Schilling, S. P. (1998). LAHARZ: GIS programs for automated mapping of lahar-inundation hazard zones. *US Geological Survey*. Open-file report 98–638.
- Schlesinger, W. H. (1990). Evidence from chronosequence studies for a low carbon-storage potential of soils. *Nature*, *348*(6298), 232–234. <https://doi.org/10.1038/348232a0>
- Shanley, C. S., Pyare, S., Goldstein, M. I., Alaback, P. B., Albert, D. M., Beier, C. M., et al. (2015). Climate change implications in the northern coastal temperate rainforest of North America. *Climatic Change*, *130*(2), 155–170. <https://doi.org/10.1007/s10584-015-1355-9>
- Sharma, A. R., & Déry, S. J. (2020). Contribution of atmospheric rivers to annual, seasonal, and extreme precipitation across British Columbia and southeastern Alaska. *Journal of Geophysical Research: Atmospheres*, *125*(9), e2019JD031823. <https://doi.org/10.1029/2019JD031823>
- Shulski, M., & Wendler, G. (2007). *The climate of Alaska*. University of Alaska Press.
- Smith, R. W., Bianchi, T. S., Allison, M., Savage, C., & Galy, V. (2015). High rates of organic carbon burial in fjord sediments globally. *Nature Geoscience*, *8*(6), 450–453. <https://doi.org/10.1038/ngeo2421>
- Smith, S. V., Renwick, W. H., Buddemeier, R. W., & Crossland, C. J. (2001). Budgets of soil erosion and deposition for sediments and sedimentary organic carbon across the conterminous United States. *Global Biogeochemical Cycles*, *15*(3), 697–707. <https://doi.org/10.1029/2000gb001341>
- Sollins, P., Spycher, G., & Topik, C. (1983). Processes of soil organic-matter accretion at a Mudfloe chronosequence, Mt. Shasta, California. *Ecology*, *64*(5), 1273–1282. <https://doi.org/10.2307/1937835>
- Spawn, S. A., & Gibbs, H. K. (2020). Global aboveground and belowground biomass carbon density maps for the year 2010 [Dataset]. ORNL DAAC. <https://doi.org/10.3334/ORNLDAAC/1763>
- Stallard, R. F. (1998). Terrestrial sedimentation and the carbon cycle: Coupling weathering and erosion to carbon burial. *Global Biogeochemical Cycles*, *12*(2), 231–257. <https://doi.org/10.1029/98gb00741>
- Swanston, D. N., Marion, D. A., Shou-Shan, F., & Yung-Huang, K. (1991). Landslide response to timber harvest in Southeast Alaska. Section 10 Man-caused problems and their control.
- U. S. Department of Agriculture Forest Service. (2018). Tongass landslide areas (feature layer) [Dataset]. U. S. Department of Agriculture, Ag Data Commons. Retrieved from <https://data.nal.usda.gov/dataset/tongass-landslide-areas-feature-layer-0>
- Van Oost, K., & Six, J. (2023). Reconciling the paradox of soil organic carbon erosion by water. *Biogeosciences*, *20*(3), 635–646. <https://doi.org/10.5194/bg-20-635-2023>
- Varnes, D. J. (1978). Slope movement types and processes. *Special Report*, *176*, 11–33.
- Vascik, B. A., Booth, A. M., Buma, B., & Berti, M. (2021). Estimated amounts and rates of carbon mobilized by landsliding in old-growth temperate forests of SE Alaska. *Journal of Geophysical Research: Biogeosciences*, *126*(11), e2021JG006321. <https://doi.org/10.1029/2021JG006321>
- Veblen, T. T., & Alaback, P. B. (1996). A comparative review of forest dynamics and disturbance in the temperate rainforests of North and South America. In R. G. Lawford, E. Fuentes, & P. B. Alaback (Eds.), *High-latitude rainforests and associated ecosystems of the west coast of the Americas: Climate, hydrology, ecology, and conservation* (pp. 173–213).
- Wang, J., Jin, Z., Hilton, R. G., Zhang, F., Li, G., Densmore, A. L., et al. (2016). Earthquake-triggered increase in biospheric carbon export from a mountain belt. *Geology*, *44*(6), 471–474. <https://doi.org/10.1130/g37533.1>
- Wang, Y., & Hsieh, Y. P. (2002). Uncertainties and novel prospects in the study of the soil carbon dynamics. *Chemosphere*, *49*(8), 791–804. [https://doi.org/10.1016/s0045-6535\(02\)00381-8](https://doi.org/10.1016/s0045-6535(02)00381-8)

- Wardle, D. A., Walker, L. R., & Bardgett, R. D. (2004). Ecosystem properties and forest decline in contrasting long-term chronosequences. *Science*, *305*(5683), 509–513. <https://doi.org/10.1126/science.1098778>
- West, A. J., Lin, C. W., Lin, T. C., Hilton, R. G., Liu, S. H., Chang, C. T., et al. (2011). Mobilization and transport of coarse woody debris to the oceans triggered by an extreme tropical storm. *Limnology & Oceanography*, *56*(1), 77–85. <https://doi.org/10.4319/lo.2011.56.1.0077>
- Yoo, K., Amundson, R., Heimsath, A. M., & Dietrich, W. E. (2005). Erosion of upland hillslope soil organic carbon: Coupling field measurements with a sediment transport model. *Global Biogeochemical Cycles*, *19*(3). <https://doi.org/10.1029/2004gb002271>
- Yoo, K., Amundson, R., Heimsath, A. M., & Dietrich, W. E. (2006). Spatial patterns of soil organic carbon on hillslopes: Integrating geomorphic processes and the biological C cycle. *Geoderma*, *130*(1–2), 47–65. <https://doi.org/10.1016/j.geoderma.2005.01.008>